INSTITUTE
FOR
AEROSPACE STUDIES

UNIVERSITY OF TORONTO

A QUANTITATIVE COMPARISON OF ACTIVE AND PASSIVE DAMPING FOR LARGE SPACE STRUCTURES

BY

FRANCIS SHEN

DOC CONTRACTOR REPORT

DOC-CR-SP-83-063

DEPARTMENT OF COMMUNICATIONS - OTTAWA - CANADA

SPACE PROGRAM

TITLE: A Quantitative Comparison of Active and Passive Damping For Large Space Structures

AUTHOR(S): Francis Shen

ISSUED BY CONTRACTOR AS REPORT NO:

PREPARED BY: Francis Shen and P.C. Hughes
Department of Aerospace Science and Engineering
University of Toronto

DEPARTMENT OF SUPPLY AND SERVICES CONTRACT NO: OSU 82-00163
HSU.36100-2-4211

DOC SCIENTIFIC AUTHORITY: F.R. Vigneron and A.H. Reynaud

CLASSIFICATION: Unclassified

DATE:

A QUANTITATIVE COMPARISON OF ACTIVE AND PASSIVE DAMPING FOR LARGE SPACE STRUCTURES

by

Francis Shen

A QUANTITATIVE COMPARISON OF ACTIVE AND PASSIVE DAMPING FOR LARGE SPACE STRUCTURES

BY

FRANCIS SHEN

DEPARTMENT OF AEROSPACE SCIENCE AND ENGINEERING

A Thesis submitted in conformity with the requirements
for the degree of Master of Applied Science
in the University of Toronto

1983

Acknowledgements

The author would like to express his sincere gratitude to Professor P. C. Hughes for his suggestion of this topic, supervision and guidance during this research, and for his critical review of this thesis.

Financial support received from the University of Toronto, Ontario Government, and Communications Research Centre is gratefully acknowledged.

Abstract

Damping has increasingly become a major issue in the control of the flexible modes of large space structures (LSS). In the past, the damping problem has been approached using two distinct techniques: active and passive damping, which have almost always been studied independently. It is therefore the intention of this report to present an interdisciplinary approach. A quantitative method for comparing active and passive damping according to weight and positivity criteria is outlined. The method assumes thruster actuators for active damping and viscoelastic material for passive damping. Each of these damping techniques is implemented by optimizing the damping performance against weight. The Mobile Communications Satellite (MSAT) is used as a model to compare active and passive damping. The results show that, in general, active damping is much more weight-cost effective and possesses better positivity qualities than passive damping. (Positivity is a term used in this report to describe robustness when the positivity concept of stability is assumed.) However, this generalization is not without exception, for example, as the filtering of the feedback signal of the active damping system increases, the weight-cost effectiveness will decrease while positivity increases. Evidently, until the design of the active system incorporates a filter for observation noise that is equal in magnitude to the disturbance noise, passive damping will not be more weight-cost effective than active damping. The results in this report cannot be complete without a good understanding of the underlying difference between active and passive damping: active damping is an on-going weight

expenditure, while passive damping is not. Thus, the major factor influencing the choice of which damping technique to implement is how much damping is required during the lifetime of the LSS. An interesting aspect concerning the positivity of the active controller is that apparently the uncertainties of the natural frequencies have a much greater effect on the system stability than the damping ratios have.

Contents

Continued...

Contents - Continued

Notation

Note: Symbols used only locally are defined when introduced.

$\underset{\sim}{A}$	system plant matrix
$\underset{\sim}{A}_\xi$	augmented system plant matrix
$\underset{\sim}{B}$	control distribution matrix
$\hat{\underset{\sim}{B}}$	$\underset{\sim}{E}^T\underset{\sim}{B}$
$\underset{\sim}{C}$	modal output matrix
$\underset{\sim}{D}$	damping matrix
$\hat{\underset{\sim}{D}}$	$\underset{\sim}{E}^T\underset{\sim}{D}\,\underset{\sim}{E}$
$\underline{e}$	$\underline{x} - \hat{\underline{x}}$
$\underset{\sim}{E}$	undamped normalized modal matrix
$\underline{E}_{\alpha i}$	i-th element eigenvector for the mode
$\underset{\sim}{F}$	feedback gain
$\underset{\sim}{H}$	observer gain
J	performance index
J_x	dynamic performance index
J_u	control effort index
$\underset{\sim}{K}$	stiffness matrix
$\underset{\sim}{K}_i$	i-th element stiffness matrix
$\underset{\sim}{L}$	compensator transfer matrix
L_α	loss factor for mode α
L_v	material loss factor
$\underset{\sim}{M}$	mass matrix
$\underset{\sim}{P}$	solution to the Riccati equation
$\underline{q}$	physical coordinates
$\underset{\sim}{Q}$	dynamical performance weighting matrix

$\underset{\sim}{Q}_k$	$E\{\underline{W}(t)\underline{W}^T(\tau)\} = \underset{\sim}{Q}_k\delta(t-\tau)$
$\underset{\sim}{R}$	control effort weighting matrix
$\underset{\sim}{R}_k$	$E\{\underline{V}(t)\underline{V}^T(\tau)\} = \underset{\sim}{R}_k\delta(t-\tau)$
$\underset{\sim}{S}_\xi$	defined in (4.39)
$\underset{\sim}{T}$	plant transfer matrix
$\underline{U}$	control vector
$\underline{V}$	observation noise
$\underline{W}$	excitation noise
$\underline{X}$	state vector
$\hat{\underline{X}}$	estimated state vector
$\underline{Y}$	output vector
δ	positivity index; impulsive function
$\hat{\delta}$	normalized delta positivity index
ζ_α	damping ratio for mode α
$\hat{\zeta}_e$	damping ratio error coefficient
$\underline{\eta}$	modal coordinates
κ	disturbance to observation noise ratio (4.31)
$\underline{\xi}$	augmented state vector (4.37)
ω_α	undamped natural frequency for mode α
$\underset{\sim}{\Omega}^2$	$\underset{\sim}{E}^T\underset{\sim}{K}\underset{\sim}{E}$

Subscripts

f	flexible modes
p	passive damping
r	rigid body modes
v	viscoelastic material

Special Notations

$\underset{\sim}{1}$	unit matrix
$(\underline{\ })$	vector
$(\underset{\sim}{\ })$	matrix
$(\ )^H$	Hermitian
$(\ )^T$	transpose
$\bar{(\ )}$	Laplace transform

1. INTRODUCTION

The advent of the Space Transportation System has made an enormous contribution to the feasibility of large space structures (LSS). However, as experience has shown (beginning with the first U.S. satellite, Explorer I), the feasibility of a spacecraft requires not only a transportation system into space, but also the stability and control of the vehicle in space. Ironically, attitude stabilization of Explorer I was lost because damping was not taken into account.

It is clear that as the sizes of space structures increase while their weights are kept to a minimum, structural flexibility becomes one of the major concerns in designing a controllable spacecraft. Indeed, this dominant characteristic has prompted much research in the area of damping technology by both structural and control engineers. However, there has been a strong tendency for the two distinct disciplines of engineering to conduct their research in two quite different directions, each with no awareness of the other.

For structural engineers, the approach is passive damping - a method of energy dissipation through the intrinsic properties of materials or passive devices. For control engineers, the approach is primarily active damping, which dissipates energy from a system through the use of sensors and actuators that require external energy input. Although some control engineers have considered passive damping, this has been limited to discrete damper devices. Understandably, the dynamics of these discrete dampers bears a remarkable resemblance to special cases of active damping. While the choice of approach has generally been dependent on the proclivities of the engineer, it is the intention of

this report to provide a quantitative comparison of active and passive damping.

In this report, the two methods are compared according to two criteria: weight and 'positivity'. The term 'positivity' refers, in this report, only to the robustness of the system using the positivity concept given in Section 5. Also, to clarify the term 'robust', this refers to the stability of a system having low sensitivity to modelling uncertainties. It should be noted that since positivity is a sufficient condition for system stability (see Section 5), positivity implies robustness, but robustness does not necessarily imply positivity. There are, of course, other criteria of interest when selecting the 'best' damping method. These include cost, complexity and spillover (which refers to the energy input or output into those modes not explicitly controlled). These, however, are beyond the scope of this report.

The strategy used to compare active and passive damping is extremely important to the outcome of selecting the 'best' damping system. The conditions under which they are compared could make an inferior technique appear to be superior; therefore it is important to appropriately select and design each damping system. The following approach is taken to assure a fair comparison.

(1) The selection of the type of damping technique that best represents each of active and passive damping is made based on comparability, hardware realizability and conventionality (Section 2).

(2) Each damping technique is designed by optimizing a performance index against weight (Section 4).

The ultimate test of any method devised is its practical application. In Section 6, the Mobile Communications Satellite (MSAT) is used as a model for LSS. Active and passive damping are applied to this structure for the purpose of comparing their damping efficiencies as to weight and positivity.

2. SELECTION OF DAMPING TECHNIQUE

Since several different techniques exist for both active and passive damping, it will be necessary to specify the damping technique used to represent each category. These damping system designs are selected on the basis of its conventionality and whether it is quantitatively comparable.

2.1 Active Damping

This category can be subdivided based on the dynamics of the control actuators. There are essentially two distinct types of actuators: force actuators and torque actuators. The former are usually produced by chemical propellant thrusters while the latter could involve a number of wheels distributed throughout the vehicle. The concept of angular momentum management has in the past been confined to the rigid part of the spacecraft, and its hardware realizability as a distribution of small wheels throughout the structure has yet to be proven. On the contrary, propellant thrusters have been used extensively for spacecraft control, and probably no significant modifications are required of them for active damping. Therefore, force actuators through the use of chemical propellant thrusters are selected to represent the performance of active damping.

2.2 Passive Damping

For passive damping, similar divisions are made based on the dynamics of the damping mechanism. The selection of a passive damping representative will also depend on how well defined these physical and geometrical parameters are. There are three categories of passive damping distinguished in this report: alternative materials, discrete damper, and viscoelastic material (VEM).

The 'alternative material' approach to passive damping augmentation uses, as the term implies, replacement of a portion of the original structure with alternative material which has better damping characteristics, while maintaining the basic material properties of the original substructure. The most promising candidates are composite materials which have shown a good strength-to-weight ratio while, under certain designs, exhibiting good damping characteristics. However, these materials are only in their initial development stage, and while research has found composite materials to have good damping characteristics, they are far from being fully documented. Therefore, this approach is not considered in this report for comparison with active damping. It should be noted that the alternative of material damping augmentation depends very much on how the composite material is designed and this requires extensive knowledge of its material properties, which is beyond the scope of this report.

The 'discrete damper' method is probably most popular with control engineers (although only a handful of them have really looked into this). The physical configuration of the hardware in these devices is not a significant concern to them, except that it is a 'mechanical fluid dashpot or electronic equivalent' [8]. There have

been several of these devices designed; however, their full employment in the space program has been limited. The usual mathematical model of these devices is envisaged as a linear-viscous mechanism. Nevertheless, the physical properties of these devices do not matter so long as they behave as their mathematical model dictates. It is interesting to note that the analysis of discrete dampers using a linear-viscous damping law is essentially the same as active damping using rate feedback and decentralized control of co-located actuators and sensors.

In any case, the discrete damper has many attractive features and, in particular, the device can be placed, with little attention to its physical configuration, at any crucial points in the spacecraft. The discrete damper usually is assumed to have the ability to selectively damp certain modes as well as alter the damping strength at will [11]. It is difficult to define the relationship between weight penalty and damping strength. The discrete dampers' physical properties and limitations are worth further investigation because these devices show great versatility (similar to active damping).

Finally, the 'viscoelastic material damping', used in this report to represent passive damping, is understandably the method most investigated by structural engineers for damping augmentation. The work done to date typically involves implementation of VEM onto a structure through such configurations as a sandwiched cantilevered beam [14, 15]. Much experimental data has been generated to support a hysteretic damping law (rather than a viscous damping law) for VEM. It should be noted that although it does more closely obey a hysteretic damping law, VEM damping is actually both frequency and temperature

dependent. However, it is assumed that modal vibrations requiring explicit control have vibrational frequencies close enough to each other that hysteretic damping can be assumed. The physical properties of VEM are well defined, making few assumptions (or guesswork) required. These conditions make VEM worthwhile for comparison with active damping. It should also be noted that VEM is basically the conventional ideal of damping where energy dissipation is achieved by applying viscous materials to the vibrating structure.

3. MATHEMATICAL MODEL

The form of the spacecraft mathematical model must be suitable for designing the damping systems considered. As well, it must be easily manipulated so that weight and positivity comparisons can readily be made. In view of these factors, the state-space form of system matrices is most satisfactory.

To begin, since finite element techniques are commonly used for modelling the dynamics of a flexible spacecraft, a dynamics model is generally given in the form

$$\underset{\sim}{M}\,\ddot{\underline{q}} + \underset{\sim}{D}\,\dot{\underline{q}} + \underset{\sim}{K}\,\underline{q} = \underset{\sim}{B}\,\underline{u} \qquad (3.1)$$

where $\underline{q}$ are the physical coordinates,

$\underset{\sim}{M}$ and $\underset{\sim}{K}$ are the mass and stiffness matrices respectively,

$\underset{\sim}{D}$ is the damping matrix,

$\underset{\sim}{B}$ is the control distribution matrix,

$\underline{u}$ is the control input.

This is normally transformed into modal coordinates by

$$\underset{\sim}{q} = \underset{\sim}{E}\,\underline{\eta} \tag{3.2}$$

resulting in the equations of motion

$$\ddot{\underline{\eta}} + \underset{\sim}{\hat{D}}\,\dot{\underline{\eta}} + \underset{\sim}{\Omega}^2\underline{\eta} = \underset{\sim}{\hat{B}}\,\underline{u} \tag{3.3}$$

where

$$\underset{\sim}{E}^T\underset{\sim}{M}\,\underset{\sim}{E} = \underset{\sim}{1}, \qquad \underset{\sim}{E}^T\underset{\sim}{K}\,\underset{\sim}{E} = \underset{\sim}{\Omega}^2$$

$$\underset{\sim}{E}^T\underset{\sim}{D}\,\underset{\sim}{E} = \underset{\sim}{\hat{D}}, \qquad \underset{\sim}{E}^T\underset{\sim}{B} = \underset{\sim}{\hat{B}}$$

Now, by partitioning

$$\underline{\eta} = \begin{bmatrix} \underline{\eta}_r \\ \underline{\eta}_f \end{bmatrix} \tag{3.4}$$

where $\underline{\eta}_r$ is the rigid body modal coordinates,

$\underline{\eta}_f$ is the flexible modal coordinates.

Equation (3.3) can be separated into the rigid body and flexible equations of motion:

$$\ddot{\underline{\eta}}_r = \underset{\sim}{\hat{B}}_r\underline{u} \tag{3.5a}$$

$$\ddot{\underline{\eta}}_f + \underset{\sim}{D}_f\dot{\underline{\eta}}_f + \underset{\sim}{\Omega}_f^2\underline{\eta}_f = \underset{\sim}{\hat{B}}_f\underline{u} \tag{3.5b}$$

where

$$\hat{\underset{\sim}{D}} = \begin{bmatrix} \underset{\sim}{0} & \underset{\sim}{0} \\ \underset{\sim}{0} & \hat{\underset{\sim}{D}}_F \end{bmatrix}, \qquad \underset{\sim}{\Omega}^2 = \begin{bmatrix} \underset{\sim}{0} & \underset{\sim}{0} \\ \underset{\sim}{0} & \Omega_f^2 \end{bmatrix}$$

and

$$\hat{\underset{\sim}{B}} = \begin{bmatrix} \hat{\underset{\sim}{B}}_r \\ \hat{\underset{\sim}{B}}_f \end{bmatrix}$$

The dimensions for the various zero matrices follow directly from the partitioning in (3.4).

The primary objective of $\hat{\underset{\sim}{B}}\underline{u}$ is often to control the rigid body modes. However, the attempt to control the rigid body modes of a flexible spacecraft almost always leads to a significant amount of undesirable spillover to the flexible modes that cannot be ignored. As described by Hughes [12], '$\hat{\underset{\sim}{B}}\underline{u}$ is often both friend and foe'. Using this analogy, the rigid body control may be considered as a foe to the flexible modes. Accordingly, (3.5) can further be broken down into the form:

$$\ddot{\underline{\eta}}_r = \hat{\underset{\sim}{B}}_r \underline{u}_r + \hat{\underset{\sim}{B}}_r \underline{u}_f \tag{3.6a}$$

$$\ddot{\underline{\eta}}_f + \hat{\underset{\sim}{D}}_f \dot{\underline{\eta}}_f + \underset{\sim}{\Omega}_f^2 \underline{\eta}_f = \hat{\underset{\sim}{B}}_f \underline{u}_r + \hat{\underset{\sim}{B}}_f \underline{u}_f \tag{3.6b}$$

where $\underline{u}_r$ is the rigid body control vector,

$\underline{u}_f$ is the flexible control vector.

For multi-input, multi-output control analysis, the state-space form of system matrices is most convenient, thus:

$$\dot{\underline{x}}_r = \underset{\sim}{A}_r \underline{x}_r + \underset{\sim}{B}_r \underline{u}_r + \underset{\sim}{B}_r \underline{u}_f \tag{3.7a}$$

$$\dot{\underline{x}}_f = \underset{\sim}{A}_f \underline{x}_f + \underset{\sim}{B}_f \underline{u}_r + \underset{\sim}{B}_f \underline{u}_f \tag{3.7b}$$

where

$$\underline{x}_r = \begin{bmatrix} \underline{\eta}_r \\ \dot{\underline{\eta}}_r \end{bmatrix}, \qquad \underline{x}_f \begin{bmatrix} \underline{\eta}_f \\ \dot{\underline{\eta}}_f \end{bmatrix}$$

$$\underset{\sim}{A}_r = \begin{bmatrix} \underset{\sim}{0} & \underset{\sim}{1} \\ \underset{\sim}{0} & \underset{\sim}{0} \end{bmatrix}, \qquad \underset{\sim}{A}_f = \begin{bmatrix} \underset{\sim}{0} & \underset{\sim}{1} \\ -\underset{\sim}{\Omega}_f^2 & -\underset{\sim}{\hat{D}}_f \end{bmatrix}$$

$$\underset{\sim}{B}_r = \begin{bmatrix} \underset{\sim}{0} \\ \underset{\sim}{\hat{B}}_r \end{bmatrix}, \qquad \underset{\sim}{B}_f = \begin{bmatrix} \underset{\sim}{0} \\ \underset{\sim}{\hat{B}}_f \end{bmatrix}$$

Using the control laws

$$\underline{u}_r = -\underset{\sim}{F}_r \underline{x} \tag{3.8a}$$

$$\underline{u}_f = -\underset{\sim}{F}_f \underline{x} \tag{3.8b}$$

where

$$\underline{x} = \begin{bmatrix} \underline{x}_r \\ \underline{x}_f \end{bmatrix} \tag{3.9}$$

and $\underset{\sim}{F}_r$ is the gain matrix for rigid body control,

$\underset{\sim}{F}_f$ is the gain matrix for flexible control,

the system may have a control block diagram given in Figure 1(a) with the following definitions:

$$\underset{\sim}{L}_r = \underset{\sim}{B}_s \underset{\sim}{F}_r \tag{3.10a}$$

$$\underset{\sim}{L}_f = \underset{\sim}{B}_s \underset{\sim}{F}_f \tag{3.10b}$$

$$\underset{\sim}{T}_r = \begin{bmatrix} (s\underset{\sim}{1}-\underset{\sim}{A}_r)^{-1} & \underset{\sim}{0} \\ \underset{\sim}{0} & \underset{\sim}{0} \end{bmatrix} \tag{3.10c}$$

$$\underset{\sim}{T}_f = \begin{bmatrix} \underset{\sim}{0} & \underset{\sim}{0} \\ \underset{\sim}{0} & (s\underset{\sim}{1}-\underset{\sim}{A}_f)^{-1} \end{bmatrix} \tag{3.10d}$$

and

$$\underset{\sim}{B}_s = \begin{bmatrix} \underset{\sim}{B}_r \\ \underset{\sim}{B}_f \end{bmatrix} \tag{3.10e}$$

The dimensions for the various zero matrices follow directly from the partitioning in (3.9).

To facilitate the positivity analysis to come in Section 5, the following assumptions are made.

(1) The control vector $\underline{u}_f$ uses only the feedback of flexible state, i.e., $\underline{u}_f = -\underset{\sim}{F}_f \underline{x}_f$.

(2) Control spillover to the rigid body modes, $\underset{\sim}{B}_r \underline{u}_f$, are not considered explicitly since it is beyond the scope of this report. However, it can be taken into account at a later stage as an independent disturbance input to the rigid body modes.

Upon these assumptions, the block diagram of Figure 1(a) can be modified to the form given in Figure 1(b) with a new definition for $\underset{\sim}{L}_f$:

$$\underset{\sim}{L}_f = \begin{bmatrix} \underset{\sim}{0} \\ \underset{\sim}{B}_f \underset{\sim}{F}_f \end{bmatrix} \tag{3.11}$$

Note that the dimension of $\underset{\sim}{F}_f$ must be adjusted accordingly.

As will be discussed in Section 5, this block diagram may also be used to describe passive damping simply by setting $\underset{\sim}{L}_f = \underset{\sim}{0}$ and modifying $\underset{\sim}{A}_f$.

Finally, to make it easier to determine $\underset{\sim}{F}_f$, as well as to facilitate weight comparison more readily, $\underset{\sim}{B}_f \underline{u}_r$ is modelled as an independent impulsive disturbance (which most accurately satisfies its analogy of a 'foe'). This model was discussed by Hughes [12] to be representative of the action of chemical propellant thrusters, and also it is a good input disturbance model which excites all frequencies. Equally important, an impulsive input has the same effect as an initial condition, which greatly simplifies the comparison process.

In order to simplify notation and since rigid body dynamics is not considered explicitly in the following sections, some notation changes are made as follows:

$$\begin{aligned} \underset{\sim}{A}_f &\to \underset{\sim}{A}, & \underset{\sim}{B}_f &\to \underset{\sim}{B} \\ \hat{\underset{\sim}{D}}_f &\to \hat{\underset{\sim}{D}}, & \underset{\sim}{\Omega}_f^2 &\to \underset{\sim}{\Omega}^2 \\ \underset{\sim}{F}_f &\to \underset{\sim}{F}, & \underline{x}_f &\to \underline{x} \end{aligned} \tag{3.12}$$

Also, it must be noted that the form of $\underset{\sim}{T}_f(s)$ and $\underset{\sim}{L}_f$ given in (3.10) and (3.11) unnecessarily complicates the positivity analysis since rigid body dynamics is not considered explicitly. Therefore, the various zero matrices of $\underset{\sim}{T}_f(s)$ and $\underset{\sim}{L}_f$, whose purpose is to accommodate addition with the rigid body system are now dropped. Thus,

$$\underset{\sim}{T}_f = (s\underset{\sim}{1} - \underset{\sim}{A}_f)^{-1} \tag{3.13a}$$

$$\underset{\sim}{L}_f = \underset{\sim}{B}_f \underset{\sim}{F}_f \qquad (3.13b)$$

4. WEIGHT CRITERION

For every component put into a spacecraft, weight is always considered to be a major factor and every attempt is made to have each component weight-cost effective. The damping system is no exception, and thus, in this section, the designs of active and passive damping are optimized against weight. Also they are set in such a way so that they can be readily compared for their weight effectiveness.

4.1 Comparison Approach

The basis for comparing the weight effectiveness of active and passive damping depend primarily on the design objectives. In this problem, the main objective is to control the flexibility of the space structure. One widely accepted measure of the flexible motion is the dynamical performance index,

$$J_x = \int_0^\infty \underline{x}^T \underset{\sim}{Q} \underline{x} \, dt \qquad (4.1)$$

where $\underset{\sim}{Q}$ is a positive semi-definite weighting matrix for the state vector of the system (3.7b). Essentially, J_x establishes a comparable medium for two very different damping methods. In other words, if J_x is the same under active control as it is under passive control, then the two systems are considered to have the same dynamical performance. The trade-off of this index against weight will allow the designer to compare the two methods of damping. It should be noted that an optimal

design must be used for each damping method in order that a valid comparison can be performed. Here, 'optimal design' refers to a control system designed with the most efficient use of weight to minimize the dynamical performance index.

4.2 Active Damping

The weight of the active controller is dependent on two distinct contributions. These are the hardware and fuel expenditures of the system. The former is relatively fixed in its weight contribution while the latter is dependent on the extent in which the active controller is used. As indicated in the previous section, the controller must be designed such that its weight is minimized against the allowable flexibility. Since the hardware weight involves such items as actuators, sensors, propellent tanks, connectors, and on-board computers, which are relatively fixed, their contribution to the total weight of the controller can be neglected in the optimization problem. Moreover, in some cases, where the existing hardware of the rigid body controller can also be used by the flexible controller, the weight contribution of the hardware could be minimal. With the omission of the hardware's weight, optimal control theory can be used easily to minimize the fuel expenditures. The optimal control performance index,

$$J = \int_0^\infty (\underline{x}^T \underset{\sim}{Q}\, \underline{x} + \underline{u}^T \underset{\sim}{R}\, \underline{u})dt \qquad (4.2)$$

conveniently incorporates the dynamic and the control effort performances for minimization using the control vector u(t) subject to:

$$\dot{\underline{x}}(t) = \underset{\sim}{A}\,\underline{x}(t) + \underset{\sim}{B}\,\underline{u}(t) \tag{4.3a}$$

$$\underline{x}(o) = \underline{x}_o \tag{4.3b}$$

For the weight of the fuel expenditure, the control effort index

$$J_u = \int_o^\infty \underline{u}^T \underset{\sim}{R}\,\underline{u}\,dt \tag{4.4}$$

must be translated to fuel weight. If the specific impulses of the thrusters and the type of fuel used by each thruster aboard the space structure are all the same, then the weighting matrix $\underset{\sim}{R}$ takes the form

$$\underset{\sim}{R} = r\underset{\sim}{1} \tag{4.5}$$

Therefore the equation to transform the control effort index to fuel expenditure is

$$M_f = (I_{sp}\,g\,r)^{-1} J_u \tag{4.6}$$

where I_{sp} is the specific impulse and g is the output thrust of the actuator. Although (4.6) measures the amount of fuel required to damp out a given disturbance, for the purpose of comparison with passive damping, the number of times this disturbance occurs during the life-time or before reservicing must also be determined. Thus, the weight of the active controller is given by

$$M_f = n_d(I_{sp}\,g\,r)^{-1} J_u \tag{4.7}$$

where n_d is the number of times the disturbance occurs. To be complete, the hardware weight, depending on the situation, should be added to give the full weight of the active controller.

4.2.1 Full-State Feedback

For full-state feedback, the optimal control vector is given by

$$\underline{u}(t) = -\underset{\sim}{F}\,\underline{x}(t) \tag{4.8}$$

where

$$\underset{\sim}{F} = \underset{\sim}{R}^{-1}\underset{\sim}{B}\,\underset{\sim}{P}$$

and $\underset{\sim}{P}$ is the symmetric positive semi-definite solution of the matrix Riccati equation

$$\underset{\sim}{A}^T\underset{\sim}{P} + \underset{\sim}{P}\,\underset{\sim}{A} - \underset{\sim}{P}\,\underset{\sim}{B}\,\underset{\sim}{R}\,\underset{\sim}{B}^T\underset{\sim}{P} + \underset{\sim}{Q} = 0 \tag{4.9}$$

The minimum cost of J subject to (4.3) is

$$J = \underline{x}_o^T\,\underset{\sim}{P}\,\underline{x}_o \tag{4.10}$$

For the dynamic performance index, the integral can be evaluated by solving P_x of the Lyapunov equation

$$\underset{\sim}{A}_c^T\,\underset{\sim}{P}_x + \underset{\sim}{P}_x\underset{\sim}{A}_c = \underset{\sim}{Q} \tag{4.11}$$

where

$$\underset{\sim}{A}_c = \underset{\sim}{A} - \underset{\sim}{B}\,\underset{\sim}{F}$$

to the idealistic state feedback. Discussed here are three methods of determining the control vector via output feedback. These methods are minimum error excitation, minimum norm excitation, and the Kalman state estimator. The minimum error excitation and minimum norm approach to optimal control are described in detail by Kosut [13], and briefly outlined here.

Minimum Error Excitation

The objective of this method is to minimize

$$I = \int_0^\infty \underline{e}_u^T \underset{\sim}{R} \underline{e}_u \tag{4.19}$$

where

$$\underline{e}_u = (\underset{\sim}{G}_c \underset{\sim}{C} - \underset{\sim}{F})\underline{x}$$

and $\underset{\sim}{G}_c$ is the gain matrix of the output feedback, where the control vector is given by

$$\underline{u} = \underset{\sim}{G}_c \underline{y} \tag{4.20}$$

The gain matrix $\underset{\sim}{G}_c$ that minimizes (4.19) is given by

$$\underset{\sim}{G}_c = \underset{\sim}{F}\ \underset{\sim}{P}_e\ \underset{\sim}{C}^T(\underset{\sim}{C}\ \underset{\sim}{P}_e\ \underset{\sim}{C}^T)^{-1} \tag{4.21}$$

where $\underset{\sim}{P}_e$ satisfies

$$(\underset{\sim}{A} - \underset{\sim}{B}\ \underset{\sim}{F})\underset{\sim}{P}_e + \underset{\sim}{P}_e(\underset{\sim}{A} - \underset{\sim}{B}\ \underset{\sim}{F})^T + \underset{\sim}{1} = \underset{\sim}{0} \tag{4.22}$$

Minimum Norm Excitation

The objective of this method is to minimize

$$\|\underset{\sim}{G}_c\underset{\sim}{C} - \underset{\sim}{F}\| \tag{4.23}$$

by the output gain matrix $\underset{\sim}{G}_c$. The norm of (4.23) is defined by Kosut to be

$$\|e_N\| = \sqrt{\sum_{i=1}^{n}\sum_{j=1}^{m} e_{ij}} \tag{4.24}$$

The resulting gain matrix under this minimization problem is

$$\underset{\sim}{G}_c = \underset{\sim}{F}\ \underset{\sim}{C}^T(\underset{\sim}{C}\ \underset{\sim}{C}^T)^{-1} \tag{4.25}$$

Kalman State Estimator

The preceding two methods determine the control vector by comparing it to the full state feedback gain matrix under certain minimization assumptions. The Kalman filtering approach, however, uses the exact gain matrix of the full state feedback system. Of course, since all of the state variables are not necessarily available (or, in some cases, a high degree of uncertainty is inherent in the state), a filtering of the output information is required. Kalman filtering is one systematic method for state estimation. Although methods such as the use of a Luenberger observer are quite popular, the resulting solution is difficult to be quantitatively described. Nevertheless, the Kalman filter is a special case of the Luenberger observer and in fact both have the form

$$\dot{\hat{\underset{\sim}{x}}}(t) = \underset{\sim}{A}\ \hat{\underset{\sim}{x}}(t) + \underset{\sim}{B}\ \underset{\sim}{u}(t) + \underset{\sim}{H}[\underset{\sim}{y}(t) - C\ \hat{\underset{\sim}{x}}(t)] \tag{4.26a}$$

$$\underline{\hat{x}}(o) = \underline{\hat{x}}_o \tag{4.26b}$$

where $\underline{\hat{x}}(t)$ is the estimated state vector.

The method for determining the matrix H is what separates the two estimators' performances. Also, state estimation by Kalman filtering is often referred to as an optimal observer. This reference owes itself to the similitude with optimal control theory. Kalman filtering requires the minimization of the dual system:

$$J_k = \int_o^\infty (\underline{e}_k \underset{\sim}{Q}_k \underline{e}_k + \underline{u}_k^T \underset{\sim}{R}_k \underline{u}_k) dt \tag{4.27}$$

subject to

$$\dot{\underline{e}}_k(t) = -\underset{\sim}{A}^T \underline{e}_k(t) - \underset{\sim}{C}^T \underline{u}_k(t) \tag{4.28}$$

$$\underline{e}_k(o) = \underline{e}_{k_o}$$

where

$$\underline{u}_k(t) = -\underset{\sim}{H}^T \underline{e}_k(t)$$

$\underset{\sim}{G}_k$ and $\underset{\sim}{R}_k$ are determined by assuming the actual system equations to be:

$$\dot{\underline{x}}(t) = \underset{\sim}{A}\, \underline{x}(t) + \underset{\sim}{B}\, \underline{u}(t) + \underline{w}(t) \tag{4.29a}$$

$$\underline{y}(t) = \underset{\sim}{C}\, \underline{x}(t) + \underline{v}(t) \tag{4.29b}$$

where $\underline{w}(t)$ and $\underline{v}(t)$ are state excitation noise and observation noise respectively and they are assumed to be uncorrelated.

If white noise is assumed, then

$$\underset{\sim}{Q}_k \delta(t - \tau) = E\{\underline{W}(t)\underline{W}^T(\tau)\} \tag{4.30a}$$

$$\underset{\sim}{R}_k \delta(t - \tau) = E\{\underline{V}(t)\underline{V}^T(\tau)\} \tag{4.30b}$$

where $E\{\cdot\}$ denotes the expected value of $\{\cdot\}$. A major advantage in using a Kalman filter is that a quantitative measure of the observer sensitivity can be described by

$$\kappa = \frac{\|\underset{\sim}{C}\ \underset{\sim}{Q}_k \underset{\sim}{C}\|}{\|\underset{\sim}{R}_k\|} \tag{4.31}$$

where κ is defined as the ratio of disturbance noise to observation noise.

Once $\underset{\sim}{Q}_k$ and $\underset{\sim}{R}_k$ are specified by the designer, the observer gain, $\underset{\sim}{H}$, can be calculated by solving for $\underset{\sim}{P}$ of the matrix Raccati equation:

$$\underset{\sim}{A}\ \underset{\sim}{P}_k + \underset{\sim}{P}_k \underset{\sim}{A}_k - \underset{\sim}{P}_k\ \underset{\sim}{B}\ \underset{\sim}{R}_k \underset{\sim}{B}^T \underset{\sim}{P}_k + \underset{\sim}{Q}_k = \underset{\sim}{0} \tag{4.32}$$

The resulting observer gain is

$$\underset{\sim}{H} = \underset{\sim}{P}_k \underset{\sim}{C}^T \underset{\sim}{R}_k^{-1} \tag{4.33}$$

Now, to analyze the performance of an optimal output feedback system, define

$$\underline{e}(t) = \underline{x}(t) - \hat{\underline{x}}(t) \tag{4.34}$$

Subtract (4.3a) from (4.26a) to give

$$\dot{\underset{\sim}{x}}(t) - \dot{\hat{\underset{\sim}{x}}}(t) = \underset{\sim}{A}[\underline{x}(t) - \hat{\underline{x}}(t)] - \underset{\sim}{H}\,\underset{\sim}{C}[\underline{x}(t) - \hat{\underline{x}}(t)] \tag{4.35}$$

or

$$\dot{\underline{e}}(t) = (\underset{\sim}{A} - \underset{\sim}{H}\,\underset{\sim}{C})\underline{e}(t) \tag{4.36}$$

Define

$$\underline{\xi} = \begin{bmatrix} \underline{x}(t) \\ \underline{e}(t) \end{bmatrix} \tag{4.37}$$

The augmented system is now given by

$$\dot{\underline{\xi}} = \underset{\sim}{A}_{\xi}\underline{\xi} \tag{4.38}$$

where

$$\underset{\sim}{A}_{\xi} = \begin{bmatrix} \underset{\sim}{A} - \underset{\sim}{B}\,\underset{\sim}{F} & \underset{\sim}{B}\,\underset{\sim}{F} \\ \underset{\sim}{0} & \underset{\sim}{A} - \underset{\sim}{H}\,\underset{\sim}{C} \end{bmatrix}$$

To calculate the dynamic performance index, consider

$$\underline{x} = \underset{\sim}{S}_{\xi}\underline{\xi} \tag{4.39}$$

where

$$\underset{\sim}{S}_{\xi} = [\underset{\sim}{1}_{n\times n} \quad \underset{\sim}{0}_{n\times n}]$$

where n is the number of flexible modes. Then (4.1) can be written as

$$J_x = \int_0^{\infty} \underline{\xi}^T \underset{\sim}{Q}_{\xi}\underline{\xi}\, dt \tag{4.40}$$

where

$$\underset{\sim}{Q}_{\xi} = \underset{\sim}{S}_{\xi}^T\, \underset{\sim}{Q}\, \underset{\sim}{S}_{\xi}$$

Therefore, the performance index can simply be calculated by solving for $\underset{\sim}{P}_{\xi}$ of the Lyapunov equation:

$$\underset{\sim}{A}_{\xi}^{T}\,\underset{\sim}{P}_{\xi} + \underset{\sim}{P}_{\xi}\underset{\sim}{A}_{\xi} = \underset{\sim}{Q}_{\xi} \tag{4.41}$$

The dynamic performance index cost is

$$J_x = \underline{\xi}_o^T\,\underset{\sim}{P}_{\xi}\underline{\xi}_o \tag{4.42}$$

where

$$\underline{\xi}_o = \begin{bmatrix} \underline{x}_o \\ \underline{e}_o \end{bmatrix}$$

For the control effort index, this can be found by calculating the total performance index and then using (4.17b) to obtain J_u.

The total performance cost can be written as

$$J = J_o + \Delta J \tag{4.43}$$

where J_o is the performance index for full state feedback,

ΔJ is the increase of performance cost due to observer dynamics.

ΔJ is given by

$$\Delta J = \int_o^{\infty} \underline{e}^T \underset{\sim}{R}_F \underline{e}\; dt \tag{4.44}$$

where

$$\underset{\sim}{R}_F = \underset{\sim}{F}^T \underset{\sim}{R}\,\underset{\sim}{F}$$

The proof of this is given in Reference 5.

Again ΔJ cost of this form can easily be calculated by solving the Lyapunov equation:

$$(\underset{\sim}{A} - \underset{\sim}{H}\,\underset{\sim}{C})^T \underset{\sim}{P}_\Delta + \underset{\sim}{P}_\Delta(\underset{\sim}{A} - \underset{\sim}{H}\,\underset{\sim}{C}) = \underset{\sim}{R}_F \tag{4.45}$$

The resulting performance cost is

$$J = \underline{x}_o^T \underset{\sim}{P}_x \underline{x}_o + \underline{e}_o^T \underset{\sim}{P}_\Delta \underline{e}_o \tag{4.46}$$

The three controllers discussed here have certain distinct properties. The minimum error excitation and minimum norm controllers do not ensure stability of the closed-loop system. In fact, it has no filtering of observation noise, which is very important when modal uncertainty and modal order truncations as well as sensors' noise are present. These two methods essentially work on the inversion of the $\underset{\sim}{C}$ matrix and in the case where there are as many state variables as output variables, the resulting control law of both minimum error excitation and minimum norm is

$$\underline{u} = \underset{\sim}{F}\,\underset{\sim}{C}^{-1}\,\underline{y} \tag{4.47}$$

This relation between the state and the output variables can easily be realized during modal order reductions.

4.3 Passive Damping

A common type of passive damping is the use of VEM where no sophisticated man-made mechanisms are employed to dissipate energy. Instead,

damping is achieved by the natural internal friction in the material. The intrinsic nature of this type of damping requires little servicing once it is implemented, except for the material's natural aging. The weight of a VEM passive damping system depends only on the amount VEM, and this amount affects the damping performance. Equally important, the optimum positioning of these materials is extremely important to effectively dissipate energy from the structure. In fact, if damping materials are placed at a section where no strain energies are distributed, then no damping enhancement will be experienced.

The problem of placing VEM on the LSS such that the control objective is optimized against weight can be posed as:

Minimize

$$J_x = \int_0^\infty \underline{x}^T \underset{\sim}{Q}\, \underline{x}\, dt \tag{4.48}$$

subject to

$$\dot{\underline{x}} = \underset{\sim p}{A}\, \underline{x}, \qquad \underline{x}(o) = \underline{x}_o, \qquad M_p = \sum_{i=1}^{p} m_i, \qquad m_i \geq 0 \tag{4.49}$$

where $\underset{\sim p}{A}$ is the system matrix (including the VEM),

M_p is the total mass of the VEM allowed,

m_i is the mass of the VEM placed at the i-th section,

p is the number of sections allowed for VEM placement.

This minimization problem has (p-1) independent variables.

To simplify this minimization problem, three assumptions are made:

(1) light hysteretic damping,

(2) $\underset{\sim}{K} + \underset{\sim V}{K} \cong \underset{\sim}{K}$ (K_V is the stiffness matrix of VEM),

(3) $\underset{\sim}{M} + \underset{\sim V}{M} \cong \underset{\sim}{M}$ (M_V is the mass matrix of VEM).

There are basically three methods for analyzing structures with distributed damping materials. These are: (1) direct frequency response method, (2) complex eigenvalue method, and (3) modal strain energy method. The method adopted in this design comparison is the modal strain energy method. The main reason for this is that, for a particular LSS, a mathematical model usually has already been developed before implementing a specific damping system. This is primarily due to the fact that an initial knowledge of the flexible modes is required in order for the designer to know how much damping augmentation is needed, and where. Furthermore, the effective use of VEM requires an insight into how strain energies are distributed and this may be achieved by an initial mathematical model. The modal strain energy method, for light damping enhancement, allows the flexibility of adding damping materials onto the structure without remodelling the whole system.

With the assumption of light damping, J_x can be simplified to the form (Reference 12)

$$J_x = \sum_{\alpha} J_{x_\alpha} \tag{4.50}$$

where

$$J_{x_\alpha} = \frac{i_\alpha^2 \, b_{\alpha_i}^2}{2L_\alpha \omega_\alpha^3} \tag{4.51a}$$

$$i_\alpha^2 = \{Q\}_{\alpha\alpha} \tag{4.51b}$$

L_α is the loss factor for mode α. The implementation of VEM will alter L_α. Nominally L_α is determined by the structure's natural damping and is related to the damping ratio by

$$L_\alpha = 2\zeta_\alpha \tag{4.52}$$

The inclusion of VEM will alter the loss factor of the α-th mode by

$$L_\alpha = 2\zeta_\alpha + L_{v_\alpha} \tag{4.53}$$

where L_{v_α} is the loss factor for mode α which is due only to the VEM implemented. To determine L_α, the modal strain energy method with the assumption of hysteretic damping gives (Reference 15):

$$L_{v_\alpha} = L_v \frac{\sum_i \underline{E}_{\alpha i}^T \underset{\sim}{K}_i \underline{E}_{\alpha i}}{\omega_\alpha^2} \tag{4.54}$$

where L_v is the material loss factor of the VEM,

$\underline{E}_{\alpha i}$ is the i-th element eigenvector for mode α,

$\underset{\sim}{K}_i$ is the i-th VEM element stiffness matrix.

The dependency of L_{v_α} on the mass of the VEM comes from $\underset{\sim}{K}_i$, thus,

$$L_{v_\alpha} = L_{v_\alpha}(m_1, m_2, \ldots, m_p) \tag{4.55}$$

The optimal design problem can now be summarized and computer coded based on the minimization problem:

Minimize

$$J_x = \sum_\alpha \frac{i_\alpha^2 \, b_{\alpha i}^2}{2(2\zeta_\alpha + L_{v_\alpha})\omega_\alpha^3} \tag{4.56}$$

subject to

$$M_p = \sum_{i=1}^{p} m_i \tag{4.57}$$

and

$$m_i \geq 0$$

To calculate J_x, the assumption of light damping allows the use of (4.56). However, this assumption can be verified by solving the Lyapunov equation:

$$\underset{\sim}{A}_p^T \underset{\sim}{P} + \underset{\sim}{P}\,\underset{\sim}{A}_p = \underset{\sim}{Q} \tag{4.58}$$

where

$$\underset{\sim}{A}_p = \underset{\sim}{A} + \underset{\sim}{A}_v$$

and

$$\underset{\sim}{A}_v = \begin{bmatrix} \underset{\sim}{0} & \underset{\sim}{0} \\ \underset{\sim}{0} & -\underset{\sim}{D}_v \end{bmatrix}$$

where

$$\underset{\sim}{D}_v = \text{Diag}\{L_{v_\alpha}\ \omega_\alpha\}$$

The subsequent cost index J_x is

$$J_x = \underline{x}_o^T \underset{\sim}{P}\,\underline{x}_o \tag{4.59}$$

J_x calculated by (4.56) should closely agree with (4.59) if the light damping assumption holds. Note that (4.59) does not assume light damping, while (4.56) does.

5. POSITIVITY CRITERION

5.1 Comparison Approach

The positivity comparison uses the theory positivity of operators to assess the relative robustness of the LSS control. A major advantage of this concept is the availability of a robust stability test which is independent of the number of, and the exact numerical values of, modal

frequencies and mode shapes. However, this robust stability test is conservative, and the conditions it demands for stability, though sufficient, are not necessary. Nonetheless, for the purpose of comparison, the 'conservativism' is assumed to be of a similar magnitude for each damping design and therefore serves as a useful comparison measure of robustness.

The positivity concept requires first the definition of 'positive realness'. This involves the transfer matrix of the system $\underset{\sim}{Z}(s)$, which must be square. This matrix is referred to as 'strictly positive real' if

(1) $\underset{\sim}{Z}(s)$ has real elements for real s,

(2) $\underset{\sim}{Z}(s)$ has elements which are analytic for $Re(s) > 0$,

(3) $\underset{\sim}{Z}(j\omega) + \underset{\sim}{Z}^{H}(j\omega)$ is positive definite for all real ω.

If the transfer matrix describing a system is strictly positive real, this implies that the system is energy dissipating. In addition, for a feedback system of the form shown in Figure 2, where $\underset{\sim}{T}(s)$ and $\underset{\sim}{L}(s)$ are square matrices, the system is asymptotically stable in the input-output sense if both transfer matrices are strictly positive real. The proof of this theorem is given in Reference 3.

This positivity concept was employed by Iwens, Benhabib, and Jackson [4] in designing a robust controller. In their work, the concept of 'embedding' was introduced in order to make use of the positivity concept for controller design. Basically, the requirement of both transfer matrices to be strictly positive real is often too restrictive and thus the embedding technique is used to alleviate this. Embedding is a block diagram transformation of the original system into a system that has the same stability characteristics. This is shown

in Appendix A. Figure 3 shows the embedding transformation of Figure 2. The embedding operator $\underset{\sim}{G}$ can be considered as a measure of how much control is required by the plant matrix or, alternatively, how stable the plant matrix is. It should be noted that embedding is a mathematical manipulation and its final goal is to use the stability theory associated with the closed-loop system Figure 2.

In Reference 4, the embedding operator $\underset{\sim}{G}$ was used in designing the controller gain, and positivity of the transfer matrices was used to check for system robustness and spillover. This report makes use of that robust test. As indicated previously, the embedding operator is a measure using positivity theory to determine how stable the system is. Therefore, by subjecting the plant matrix to varying degrees of modal errors, one can determine how stable the system is via the embedding operator. Using the embedding operator as a quantitative measure of robustness, a comparison can be made between different damping designs.

The determination of $\underset{\sim}{G}$ requires the definition of a positivity index:

$$\delta(\omega) = \lambda_{min}\left\{\frac{1}{2}\left[\underset{\sim}{T}(j\omega) + \underset{\sim}{T}^{H}(j\omega)\right]\right\} \tag{5.1}$$

where $\lambda_{min}\{\cdot\}$ is the smallest eigenvalue $\{\cdot\}$. Also define

$$\delta_{min} = \min_{0<\omega<\infty}\{\delta(\omega)\} \tag{5.2}$$

One form of $\underset{\sim}{G}$ can be

$$\underset{\sim}{G} = -\delta_{min}\underset{\sim}{1} \tag{5.3}$$

This embedding operator will set the plant matrix positive at the expense of the controller. The transformed system for stability analysis is

$$\tilde{\underset{\sim}{T}} = \underset{\sim}{T} + \underset{\sim}{G} \tag{5.4a}$$

$$\tilde{\underset{\sim}{L}} = (\underset{\sim}{1} - \underset{\sim}{L}\,\underset{\sim}{G})^{-1}\underset{\sim}{L} \tag{5.4b}$$

A modal data error of the plant matrix may cause a change to the embedding operator. By normalizing the change of the positivity index to modal errors, a comparison can be made of the sensitivity of the damping design to modal data.

Define a normalized delta positivity index

$$\hat{\delta} = (\delta_e - \delta_o)/\delta_o \tag{5.5}$$

where δ_e is the positivity index with error in the modal data,

δ_o is the positivity index without error in the passive damping,

$\underset{\sim}{T}_f$ is the plant matrix inclusive of the passive damping system,

and thus the matrix associated with $\underset{\sim}{T}_f$ is $\underset{\sim}{A}_p$. In addition, $\underset{\sim}{L}_f$ is set to a null matrix for passive damping. The embedding technique transforms the block diagram of Figure 1a into Figure 4. Therefore, the comparison of robustness is based upon the penalty that $\underset{\sim}{L}_r$ has to pay in order to maintain similar positivity of the nominal system when modal data error is encountered. It should be noted that the flexible controller's spill-over to the rigid body modes is neglected for the reasons given in Section 3.

5.2 Active Damping

5.2.1 Full-State Feedback

To calculate the positivity index of the full state feedback system, consider the block diagram of Figure 4. The embedding operator is determined by the characteristics of the feedback loop having the transfer matrix

$$\underset{\sim}{T}_{fc} = (\underset{\sim}{1} + \underset{\sim}{T}_f\underset{\sim}{L}_f)^{-1}\underset{\sim}{T}_f \tag{5.8}$$

For the output feedback system

$$\underset{\sim}{T}_f = (s\underset{\sim}{1} - \underset{\sim}{A})^{-1} \tag{5.9a}$$

$$\underset{\sim}{L}_f = \underset{\sim}{B}\ \underset{\sim}{F} \tag{5.9b}$$

The resulting plant matrix with flexible control can be determined by substituting (5.9) into (5.8)

$$\underset{\sim}{T}_{fc} = [\underset{\sim}{1} + (s\underset{\sim}{1} - \underset{\sim}{A})^{-1}\underset{\sim}{B}\ \underset{\sim}{F}]^{-1}(s\underset{\sim}{1} - \underset{\sim}{A})^{-1} \tag{5.10}$$

Simplifying gives

$$\underset{\sim}{T}_{fc} = (s\underset{\sim}{1} - \underset{\sim}{A} + \underset{\sim}{B}\ \underset{\sim}{F})^{-1} \tag{5.11}$$

As prescribed by Equation (5.1), the positivity index is calculated by

$$\delta(\omega) = \lambda_{min}\left\{\frac{1}{2}\left[\underset{\sim}{T}_{fc}(j\omega) + \underset{\sim}{T}^{H}_{fc}(j\omega)\right]\right\} \tag{5.12}$$

Substituting (5.11) gives

$$\delta(\omega) = \lambda_{min}\left\{\frac{1}{2}\,(j\omega\underset{\sim}{1} - \underset{\sim}{A} + \underset{\sim}{B}\,\underset{\sim}{F})^{-1} + (j\omega\underset{\sim}{1} - \underset{\sim}{A} + \underset{\sim}{B}\,\underset{\sim}{F})^{-H}\right\} \qquad (5.13)$$

For ease in computer coding, this can be greatly simplified to

$$\delta(\omega) = \frac{1}{2}\,\lambda_{min}\{-\underset{\sim}{N}\,\underset{\sim}{A}_c - (\underset{\sim}{N}\,\underset{\sim}{A}_c)^T + j\omega(\underset{\sim}{N}^T - \underset{\sim}{N})\} \qquad (5.14)$$

where

$$\underset{\sim}{N} = (\omega^2\underset{\sim}{1} - \underset{\sim}{A}_c\underset{\sim}{A}_c)^{-1}$$

$$\underset{\sim}{A}_c = \underset{\sim}{A} - \underset{\sim}{B}\,\underset{\sim}{F}$$

See Appendix B for this simplification.

5.2.2 Output Feedback

The positivity index of the minimum-error or minimum-norm excitation methods is similar to that of the full state feedback. The difference is simply

$$\underset{\sim}{L}_f = \underset{\sim}{B}\,\underset{\sim}{F}\,\underset{\sim}{P}_e\underset{\sim}{C}^T(\underset{\sim}{C}\,\underset{\sim}{P}_e\underset{\sim}{C}^T)^{-1}\underset{\sim}{C} \qquad (5.15)$$

for minimum error excitation and

$$\underset{\sim}{L}_f = \underset{\sim}{B}\,\underset{\sim}{F}\,\underset{\sim}{C}^T(\underset{\sim}{C}\,\underset{\sim}{C}^T)^{-1}\underset{\sim}{C} \qquad (5.16)$$

for minimum norm excitation.

Therefore, the positivity index is the same as (5.14) except for the modifications to $\underset{\sim}{A}_c$. For minimum error excitation,

$$\underset{\sim}{A}_c = \underset{\sim}{A} - \underset{\sim}{B}\ \underset{\sim}{F}\ \underset{\sim}{P}_e\underset{\sim}{C}^T(\underset{\sim}{C}\ \underset{\sim}{P}_e\underset{\sim}{C}^T)^{-1}\underset{\sim}{C} \tag{5.17}$$

and for minimum norm excitation

$$\underset{\sim}{A}_c = \underset{\sim}{A} - \underset{\sim}{B}\ \underset{\sim}{F}\ \underset{\sim}{C}^T\ (\underset{\sim}{C}\ \underset{\sim}{C}^T)^{-1}\underset{\sim}{C} \tag{5.18}$$

When an observer is used such as a Kalman filtering state estimator, the problem becomes slightly more complex. Proceeding as the full state feedback problem, the transfer matrices T_f and L_f are

$$\underset{\sim}{T}_f = (s\underset{\sim}{1} - \underset{\sim}{A})^{-1} \tag{5.19a}$$

$$\underset{\sim}{L}_f = \underset{\sim}{B}\ \underset{\sim}{F}(s\underset{\sim}{1} - \underset{\sim}{A} + \underset{\sim}{B}\ \underset{\sim}{F} + \underset{\sim}{H}\ \underset{\sim}{C})^{-1}\underset{\sim}{H}\ \underset{\sim}{C} \tag{5.19b}$$

The derivation of $\underset{\sim}{L}_f$ is a simplification of the block diagram of Figure 5. It should be noted that these transfer matrices apply not only to Kalman filtering observers but also to the Luenberger type observers.

Equation (5.19) leaves a rather complex system for calculating the positivity index where the plant matrix with flexible control is given by

$$\underset{\sim}{T}_{fc} = [s\underset{\sim}{1} - \underset{\sim}{A} + \underset{\sim}{B}\ \underset{\sim}{F}(s\underset{\sim}{1} - \underset{\sim}{A} + \underset{\sim}{B}\ \underset{\sim}{F} + \underset{\sim}{H}\ \underset{\sim}{C})^{-1}\underset{\sim}{H}\ \underset{\sim}{C}]^{-1} \tag{5.20}$$

To overcome this unnecessary complexity, consider the augmented system discussed in Section 4.3.2, except that here, instead of using the initial condition as the disturbance in the system equations, impulsive inputs are used which have the same effect. Therefore, by setting $\underline{\xi}_o$ to zero, the augmented system is then given by

$$\dot{\underline{\xi}} = \underset{\sim}{A}_{\xi}\underline{\xi} + \underset{\sim}{S}_{\xi}^{T}\,\underline{f}_r \tag{5.21}$$

$$\underline{\xi}(o) = \underline{0}$$

The transfer function for this augmented system is

$$\underset{\sim}{T}_{\xi} = (s\underset{\sim}{1} - \underset{\sim}{A}_{\xi})^{-1}\underset{\sim}{S}_{\xi}^{T} \tag{5.22}$$

where $\underline{f}_r$ is the input and $\underline{\xi}$ is the output.

Since $\underline{x} = \underset{\sim}{S}_{\xi}\underline{\xi}$, then the transfer matrices $\underset{\sim}{T}_{fc}$ is related to $\underset{\sim}{T}_{\xi}$ by

$$\underset{\sim}{T}_{fc} = \underset{\sim}{S}_{\xi}^{T}\,\underset{\sim}{T}_{\xi} \tag{5.23}$$

or

$$\underset{\sim}{T}_{fc} = \underset{\sim}{S}_{\xi}(s\underset{\sim}{1} - \underset{\sim}{A}_{\xi})^{-1}\underset{\sim}{S}_{\xi}^{T} \tag{5.24}$$

As can be seen, the form of $\underset{\sim}{T}_{fc}$ given by (5.24) is much simpler than (5.19b), especially when evaluating the positivity index. Using (5.24) and substituting it into (5.12) the positivity index is

$$\delta(\omega) = \frac{1}{2}\,\lambda_{min}\{\underset{\sim}{S}_{\xi}(j\omega\underset{\sim}{1} - \underset{\sim}{A}_{\xi})^{-1}\underset{\sim}{S}_{\xi}^{T} + \underset{\sim}{S}_{\xi}(j\omega\underset{\sim}{1} - \underset{\sim}{A}_{\xi})^{-H}\underset{\sim}{S}_{\xi}^{T}\} \tag{5.25}$$

after noting that $(S_{\xi}^T)^H = S_{\xi}$. Upon simplification for computer coding, the positivity index can be evaluated by

$$\delta(\omega) = \frac{1}{2}\lambda_{min}\{S_{\xi}[-N_{\xi}A_{\xi} - (N_{\xi}A_{\xi})^T + j\omega(N_{\xi}^T - N_{\xi})]S_{\xi}^T\} \qquad (5.26)$$

where

$$N_{\xi} = (\omega^2 1 + A_{\xi}A_{\xi})^{-1}$$

See Appendix B for this simplification.

5.3 Passive Damping

As discussed in Section 5.1, the block diagram of Figure 4 represents a passive damping system by setting $L_f = 0$ and including the VEM dynamics in T_{fc}. As such, the positivity index can be calculated by

$$\delta(\omega) = \frac{1}{2}\lambda_{min}\{(j\omega 1 - A_p)^{-1} + (j\omega 1 - A_p)^{-H}\} \qquad (5.27)$$

where A_p is defined in Section 4.3.

Again this can be simplified (Appendix B) to

$$\delta(\omega) = \frac{1}{2}\lambda_{min}\{-N_pA_p - (N_pA_p)^T + j\omega(N_p^T - N_p)\} \qquad (5.28)$$

where

$$N_p = (\omega^2 1 + A_pA_p)^{-1}$$

6. APPLICATION OF THE COMPARISON METHOD TO MSAT

A comparison of active and passive damping for the Operational Mobile Communication Satellite (MSAT) shown in Figure 6 is conducted

in this section to demonstrate the quantitative method just outlined in this report. The MSAT is a relatively flimsy structure, composed of a 44-meter diameter dish antenna, a 44-meter supporting tower boom, a cross boom, a solar array and a main bus. Of all the main structural components, only the bus can be considered rigid. Thus, the MSAT model poses a good example of a flexible space structure for damping design analyses. It should be noted that the availability of this rather comprehensive mathematical model of the vehicle's dynamics (developed by P. C. Hughes and G. B. Sincarsin of Dynacon Enterprises Ltd.) makes possible this quantitative comparison of damping designs. The basic dynamic objective of the MSAT while orbiting the Earth is to maintain the focus of the paraboloid reflector nominally at the feeder horns located on the bus while aiming the communication beam at its target on Earth. It was suggested that some damping augmentation should be implemented in order to upgrade its structural integrity.

Different approaches to damping augmentation as outlined in this report were applied to the MSAT for comparison. The various methods of damping augmentation were computer coded, but are quite complex to be reused. This is because the comparison involves many varying input design parameters, and the results of one program are required by several other programs. Also, in the intermediate stages of some of the programs, numerous data files were generated in order to reduce repetitive computations. The ultimate reason for all this complexity was to minimize the computing cost. Therefore, a listing of the programs used is not provided.

6.1 MSAT's Mathematical Model

The MSAT had originally a total of 108 modes which were reduced to a design model of four flexible modes and eight rigid body modes. The comparison uses this model. Since the analysis only concerns four flexible modes, the output vector (in physical coordinates) was chosen to be

$$\underline{y} = \text{col}(\delta_1, \delta_2, \alpha_1, \alpha_2) \tag{6.1}$$

δ_1 and δ_2 are relative displacement of tower tip to tower root, and α_1 and α_2 are relative angular displacement of the reflector with respect to frame fixed at tower root. These physical coordinates were chosen because they were completely independent of the eight rigid body modes and are pervasive for all four flexible modes.

The modal output matrix $\hat{\underset{\sim}{C}}$ is

$$\hat{\underset{\sim}{C}} = \begin{bmatrix} -1.756\text{x}10^{-3} & -3.172\text{x}10^{-6} & 2.786\text{x}10^{-3} & -2.075\text{x}10^{-3} \\ 2.418\text{x}10^{-6} & -5.019\text{x}10^{-4} & -1.230\text{x}10^{-6} & -4.650\text{x}10^{-7} \\ 4.200\text{x}10^{-6} & 3.425\text{x}10^{-3} & -2.497\text{x}10^{-6} & 2.209\text{x}10^{-6} \\ 5.736\text{x}10^{-5} & 1.776\text{x}10^{-6} & -1.050\text{x}10^{-3} & -5.249\text{x}10^{-4} \end{bmatrix} \tag{6.2}$$

The natural frequencies of the design modes are:

$$\omega_\alpha = 0.124,\ 0.240,\ 0.341,\ 0.556 \quad \text{rad/sec} \quad (\alpha = 1, 2, 3, 4) \tag{6.3}$$

A 1% damping was assumed in each of the substructures [10] and the modal damping matrix is:

$$\hat{\underset{\sim}{D}} = \begin{bmatrix} 1.846\text{x}10^{-3} & & & \\ 2.519\text{x}10^{-6} & 3.409\text{x}10^{-3} & & \text{Symmetric} \\ -1.700\text{x}10^{-3} & -6.900\text{x}10^{-6} & 1.711\text{x}10^{-2} & \\ 1.237\text{x}10^{-3} & 5.243\text{x}10^{-6} & -6.647\text{x}10^{-3} & 1.109\text{x}10^{-2} \end{bmatrix} \tag{6.4}$$

From a geometrical calculation of the relative importance of roll, pitch and yaw as well as internal flexibility, the modal weighting matrix was calculated to be

$$\hat{\underset{\sim}{Q}} = \begin{bmatrix} 2.014\text{x}10^{-6} & & & \\ 8.746\text{x}10^{-9} & 1.115\text{x}10^{-6} & & \text{Symmetric} \\ -8.075\text{x}10^{-6} & -4.195\text{x}10^{-8} & 4.247\text{x}10^{-5} & \\ 4.569\text{x}10^{-6} & 2.283\text{x}10^{-8} & -2.203\text{x}10^{-5} & 1.176\text{x}10^{-5} \end{bmatrix} \tag{6.5}$$

Using the light damping assumption, the matrix of (6.4) and (6.5) can be simplified to only eight modal parameters. They are the damping ratios, ζ_α, and 'modal involvement indices', i_α, for the four flexible modes,

$$\zeta_\alpha = (7.421,\ 7.116,\ 5.013,\ 15.374) \times 10^{-3} \tag{6.6}$$

$$(\alpha = 1, 2, 3, 4)$$

$$i_\alpha = (1.419,\ 1.056,\ 0.105,\ 6.517) \times 10^{-3} \tag{6.7}$$

The actuators aboard the MSAT consist of a total of eight thrusters, three reaction wheels in the bus, and two torquers at the reflector hub. The modal control distribution matrix, $\hat{\underset{\sim}{B}}$, of this arrangement is given in Table 1. To summarize the mathematical model used, the system in first-order assumes (note that this only includes the

flexible modes)

$$\underset{\sim}{x} = \begin{bmatrix} \underline{\eta} \\ \dot{\underline{\eta}} \end{bmatrix} \tag{6.8}$$

and the resulting system equation as prescribed in (4.3) and with the following matrix definition:

$$\underset{\sim}{A} = \begin{bmatrix} \underset{\sim}{0} & \underset{\sim}{1} \\ -\underset{\sim}{\Omega}^2 & -\underset{\sim}{\hat{D}} \end{bmatrix}, \qquad \underset{\sim}{B} = \begin{bmatrix} \underset{\sim}{0} \\ \underset{\sim}{\hat{B}} \end{bmatrix}$$

The associated $\underset{\sim}{Q}$ and $\underset{\sim}{C}$ for the MSAT have the form:

$$\underset{\sim}{Q} = \begin{bmatrix} \underset{\sim}{\hat{Q}} & \underset{\sim}{0} \\ \underset{\sim}{0} & \underset{\sim}{0} \end{bmatrix}, \qquad \underset{\sim}{C} = [\underset{\sim}{\hat{C}} \quad \underset{\sim}{0}]$$

The dimensions for the various zero matrices follow directly from the partitioning in (6.8).

6.2 Damping Designs

The type of damping designs that are considered here for the MSAT are active damping with full state feedback and with output feedback, and passive damping using VEM. The mathematical design approaches were all outlined in Sections 4 and 5. All the design methods were used explicitly from these sections except for minimum error and minimum norm excitation method. This is because these two methods do not guarantee stability and have no filtering of the output noise as

demonstrated when $\underset{\sim}{C}$ is square in Section 4.3.2.

6.2.1 Active Damping

As outlined in Section 4, two situations of active controls are considered: active control with full state feedback and with output feedback. Linear quadratic optimal control theory was applied to both these situations. For active damping with full state feedback, the design of the controller involves solving (4.9) and then substituting $\underset{\sim}{P}$ into (4.8). All the matrices were as prescribed in Section 6.1. Only the $\underset{\sim}{R}$ matrix needs to be determined, but as discussed in Section 4.2, by varying r, defined by (4.5) will give a range of M which will arrive at a relation between fuel expenditure and dynamical performance. For active damping with output feedback, the design of the controller is similar to the full state feedback case except that instead of the feedback vector being $\underset{\sim}{x}$ in (4.8) it is $\underset{\sim}{\hat{x}}$. $\underset{\sim}{\hat{x}}$ was calculated by setting κ defined in (4.31) which in turn gives $\underset{\sim}{Q}_k$ and $\underset{\sim}{R}_k$ of (4.32) for the observer gain given by (4.33).

In order to use Equation (4.7), several parameters were assumed: I_{sp} = 500 N-s, δ = 0.1N, and $n_d = 10^6$. The first two parameters were determined based on the use of a low thrust monopropellant hydrazine thruster system while n_d, the number of times the disturbance occurs during the lifetime of the LSS, was selected to represent a long duration spacecraft.

6.2.2 Passive Damping

Some internal structural modelling is required for passive damping design and this would depend on where the VEM is to be applied. The

aim of having this internal structural model is to use Equation (4.54) which requires the strain energy distribution. The optimal application locations for the VEM depend on three aspects. They are: the design objective; the strain energy distribution; and the disturbances. An insight into some of these aspects can greatly simplify the problem. Considering the objective of the control problem, the effect of flexibility of the MSAT renders a major concern, the maintenance of correct positioning of the reflector and the feeder horns. This suggests that the tower-cross boom is a good place to distribute the damping material. Once the problem of applying the VEM has been narrowed down to the tower-cross boom structure, a detailed modelling of this structure is required to ascertain a strain energy distribution. Since a model of the tower-cross boom was available in detail through Reference 10, the construction of the finite element model may simply follow in this manner.

To begin with, the tower-cross boom was modelled as a four-element rod structure as shown in Figure 7(a). The dynamics of this structure can be completely described by $\underline{q}_i$, $\underline{\alpha}$, $\underline{\delta}$, and $\underline{w}_b$ and $\underline{\theta}_b$, where $\underline{w}_b$ and $\underline{\theta}_b$ are three translational and three rotational coordinates of the main bus, respectively, and $\underline{q}_i$ is the twoer's internal coordinates. $\underline{\alpha}$ and $\underline{\delta}$ are three relative angular displacement and three relative displacement of tower tip to tower root, respectively. This gives a total of 26 coordinates. The strain energy that is distributed over this structure for the flexible controller design only considers the four flexible modes. Thus, the eigenvectors of these 4 modes were required, and they were transformed to physical coordinates of the tower relative to the inertial space. This transformation was devised by Reference 10, page 35,

and the transformation has the relation

$$\underline{q}_t = \underset{\sim}{S}_t \text{col}\{\underline{w}_b, \underline{\theta}_b, \underline{\delta}, \underline{\alpha}, \underline{q}_i\}$$

where $\underset{\sim}{S}_t$ is the transformation matrix, or the selection matrix as referred to by the reference. It should be noted that $\underline{w}_b$ and $\underline{\theta}_b$ are related to $\underline{w}_t$ and $\underline{\theta}_t$ (translation and rotation at the tower root) by a simple rotation matrix. With the 32 tower coordinates $\underline{q}_t$, the eigenvectors are further broken down into elemental eigenvectors, $\underline{E}\alpha_i$. To reiterate, the purpose of this is to facilitate the use of Equation (4.54) or, more precisely, to determine the modal strain energy distribution over the tower-cross boom structure. This distribution is given in Table 2 for the four-element model of the twoer-cross boom structure.

Several input parameters were assumed, as follows:

(1) Effective diameter of tower-cross boom = 1.5m.

(2) Density of the VEM = 1.5×10^3 kg/m^3.

(3) Young's modulus = 6.2×10^6 N/m^2.

(4) Shear modulus = 2.07×10^6 N/m^2.

(5) Material loss factor = 1.3.

(6) Equal impulsive input from all eight thrusters fired independently.

The basic algorithm used to determine the optimal placement of the VEM follows the flow diagram shown in Figure 8. The result of this optimization yielded an arrangement where the damping material is most weight-cost effective when placed on element one, Figure 7(b). However, this result is based on an equal impulsive input by the eight thrusters. In the case where the disturbance is only an impulsive input generated

by thruster two, the most effective placement of the damping material was found to be on element two.

6.3 Damping Design Comparisons

Once the damping systems were designed, the next step was to compare their damping effectiveness based on the two criteria of weight and positivity. The candidate designs were subjected to an impulsive disturbance fired independently from the eight thrusters on board the spacecraft. This was felt to best approximate the type of disturbances that may be encountered by the structure, since there is no reason to single out any one particular thruster or combination of them. It should be noted that the optimal design of the passive damping system is dependent on the type of disturbances, while the active damping system is not (at least so far as the control law is concerned).

6.3.1 Weight Criterion

Figure 9 shows a weight comparison of three damping designs — passive, active with full state feedback, and active with output feedback. In this plot, it shows clearly that active damping with full state feedback gives the best dynamic performance to weight applied. Passive damping appears to be the least effective, but it cannot be stressed strongly enough that this plot assumes no hardware weight contribution for the active damping analysis and no credit is given the passive damping for damping the 'higher modes'. The active system with an observer designed for noise level of $\kappa = 10^3$ shown in the same figure, agrees with the physical mechanics of noise filtering. That is, its control performances are damped to account for the possible observation noise; thus the structural

damping is less weight-cost effective as shown in this figure. This is further demonstrated in Figures 10 and 11, where the controller was designed for varying levels of observation noise: $\kappa = 10$ and $\kappa = 2$. Evidently, as κ decreases (κ is inversely proportional to the observer noise), the dynamical performance index will reach a saturation point much earlier at which increased fuel expenditure will not improve damping. This is shown most clearly by Figure 11, where a controller designed for a low ratio of disturbance noise to observation noise exhibits a saturation point quite abruptly at M = 2.5 kg.

6.3.2 Positivity Criterion

A logical common denominator for comparing the robustness of several damping designs is to have a common weight for each design. This way, one can determine which damping system is most robust for a given weight. A common weight of 10 kg was chosen and Figure 12 shows $\hat{\delta}$ as a function of the error coefficient for $\hat{\zeta}_e$, defined as $\hat{\zeta}_e = \Delta\zeta_\alpha/\zeta_\alpha$. This plot compares the passive, active with full state feedback, and active with output feedback ($\kappa = 20$) damping systems. Surprisingly, the passive damping design shows more sensitivity to the modal data ζ_α than active damping. However, the behaviour of the active damping design agrees with intuition in that the more filtering of the output vector, the less sensitivity to modal data, and hence the more robustness. In fact, this was investigated further; Figure 13 shows that as κ decreases the robustness increases (other things being equal).

To consider errors in the modal data ω_α, Figure 14 plots $\hat{\delta}$ versus $\hat{\omega}_e$ which is defined as $\hat{\omega}_e = \Delta\omega/\omega_1$. This plot is complementary to Figure 12: it compares the positivity of three systems: passive, active with

full state feedback, and active with output feedback ($\kappa = 20$). Again the passive damping design shows more sensitivity to modal data errors. Similarly, positivity is observed to increase when the observer incorporates a filtering process as shown in Figure 15. This filtering process is shown to increase positivity as the strength of the filter increases. This effect of filtering on positivity is further confirmed by Figures 16 and 17, where the weight of the fuel expenditure was set at 5 kg.

There are several noteworthy characteristics of the plots in Figures 9-17:

(1) It appears that for active damping where a filter is incorporated, there exists a saturation value for J_x which is not zero, but which increases as κ decreases.

(2) The relation between $\hat{\delta}$ and $\hat{\zeta}_e$ is rather linear while that between $\hat{\delta}$ and $\hat{\omega}_e$ is not.

(3) The variation of $\hat{\delta}$ with $\hat{\omega}_e$ is about an order of magnitude greater than the variation of $\hat{\delta}$ with $\hat{\zeta}_e$. This suggests, for example, a 5% error in ω_α may be as important as a 50% error in ζ_α.

7. CONCLUSIONS

A quantitative method for comparing active and passive damping according to weight and positivity criteria has been presented. The method assumes thruster actuators for active damping and viscoelastic material for passive damping. Each of these damping techniques has been implemented by optimizing the damping performance against weight.

This method was applied to the MSAT model and the results of the comparison are shown in Figures 9 to 17. The following major conditions should be kept in mind when examining these figures:

(1) The weight comparison was made based on impulsive disturbances from all eight thrusters firing independently for a million times. Note that this is to model the lifetime disturbances imposed by the rigid body controller on the flexible system.

(2) The weight of the active damping system is calculated with the inclusion of only the lifetime fuel expenditures used. Therefore, it should be clear that the hardware weight is not accounted for.

(3) The positivity concept is a conservative approach to stability analysis.

The results of this comparison show active damping with full state feedback to give much better damping performance for a given weight than does passive damping. This is accompanied also with active damping being superior in positivity when compared to passive damping. Of course, full state feedback is an idealized situation where the entire state is available and without noise. Although this is an unrealistic situation, it defines a useful reference point for the best damping-performance-to-fuel-weight that the active approach can achieve. Having this design in perspective, a more realistic active controller was designed and compared with passive damping. As expected, the more filtering was incorporated into the controller, the less effective was the damping performance, but the more robust the system became. Even with filtering of the feedback vector, it appears that for the MSAT, active damping is much more efficient per unit weight unless the disturbance (caused by rigid body control) is

of equal magnitude to observation noise. As Figure 11 suggests, only for a relatively low disturbance noise/observation noise ratio ($\kappa = 2$), passive damping shows a weight-cost benefit when the damping systems are allowed to weigh more than 7.5 kg. In general, however, it would appear that for moderate filtering in the control system, active damping is better under the criteria considered. As well, if a system of thrusters such as those on MSAT are already in existence for rigid body control, then only an adjustment in the controller's gain would greatly enhance damping. This is because of the exponential drop of J_x (increase in damping performance) that occurs for small additional fuel expenditures. An interesting robustness aspect that should be noted is that uncertainties in natural frequencies have a much greater effect on system stability than uncertainties in damping ratios.

In applying this comparison method, one must keep in mind the underlying nature of active and passive damping. Active damping is an on-going weight expenditure, while passive damping is an initial, nonrecurring weight investment. With this understanding, lifetime becomes a major factor in the decision.

Finally, this method was developed with the intention to place the trade-offs of active and passive damping on an objective level. As with all non-trivial design problems, many criteria exist and in most cases, it is not possible to quantify them all. This problem is no exception, and final decisions will still require ample engineering judgement.

REFERENCES

1. Athans, M., Levine, W. S., "On the Determination of the Optimal Constant Output Feedback Gains for Linear Multivariable Systems", IEEE Transactions on Automatic Control, Vol. 15, pp. 44-48, Feb. 1970.
2. Balas, M. J., "Active Control of Flexible Systems", AIAA Symposium on Dynamics and Control of Large Flexible Spacecraft", Blacksburg, Virginia, June 1977.
3. Benhabib, R. J., Iwens, R. P., Jackson, R. L., "Stability of Large Space Structure Control Systems Using Positivity Concepts", J. Guidance and Control, Vol. 4, No. 5, Sept-Oct. 1981.
4. Benhabib, R. J., Iwens, R. P., Jackson, R. L., "A Unified Approach to the Design of Large Space Structure Control Systems", Joint Automatic Conference, August 1980.
5. Bongiorno, J., Youla, D., "On Observers in Multi-Variable Control Systems", Int. Jour. Control, Vol. 8, pp. 221-243, 1968.
6. Croopnick, S. R., Lin, Y. H., Strunce, R. R., "A Survey of Automatic Control Techniques for Large Space Structures", The Charles Stark Draper Laboratory, Massachusetts, 1979.
7. Graham, W. B., "Material Damping and Its Role in Linear Dynamic Equations", UTIAS Review No. 36, March 1973.
8. Henderson, T. C., "Damping Augmentation for Large Space Structures", The Charles Stark Draper Laboratory, Massachusetts, 1977.
9. Hughes, P. C., "MSAT Structural Flexibility and Control Assessment", Dynacon Report MSAT-1, March 1981.

10. Hughes, P. C., Sincarsin, G. B., "MSAT Structural Dynamics Model for Control System Evaluation", Dynacon Report MSAT-4, March 1982.

11. Hughes, P. C., "Modeling of Energy Dissipation (Damping) in Flexible Space Structures", Dynacon Report MSAT-6, March 1982.

12. Hughes, P. C., "Modal Cost Analysis as an Aid in Control System Design for Large Space Structures", Proceedings of the Symposium on Large-Scale Engineering Systems, Taiwan, Dec. 26-28, 1981.

13. Kosut, R., "Suboptimal Control of Linear Time-Invariant Systems Subject to Control Structure Constraints", IEEE Transactions on Automatic Control, Vol. 15, No. 5, Oct. 1970.

14. Parin, M. L., "Material Property Measurements Aid Data Reduction Resonant Beam Measurement Techniques", Vibration Damping Short Course Notes of University of Dayton, November 1979.

Table 1

Modal Control Distribution Matrix ($\hat{B}^T$)

Actuator No.	Mode			
	1	2	3	4
1	-8.282×10^{-7}	-9.888×10^{-4}	8.859×10^{-7}	-1.407×10^{-6}
2	-5.856×10^{-4}	2.133×10^{-7}	-3.964×10^{-4}	-3.743×10^{-4}
3	1.157×10^{-3}	5.812×10^{-6}	-5.932×10^{-3}	3.110×10^{-3}
4	-5.553×10^{-4}	-1.500×10^{-6}	8.518×10^{-4}	1.688×10^{-5}
5	-2.199×10^{-6}	-2.577×10^{-3}	1.731×10^{-6}	-8.184×10^{-7}
6	6.530×10^{-3}	-3.368×10^{-3}	-2.485×10^{-2}	1.358×10^{-2}
7	-3.478×10^{-3}	3.370×10^{-3}	2.639×10^{-2}	-1.328×10^{-2}
8	3.488×10^{-3}	3.419×10^{-3}	-2.653×10^{-2}	1.336×10^{-2}
9	-6.539×10^{-3}	-3.421×10^{-3}	2.499×10^{-2}	-1.363×10^{-2}
10	-1.039×10^{-2}	1.806×10^{-2}	4.926×10^{-6}	-1.654×10^{-4}
11	-1.027×10^{-2}	-1.806×10^{-2}	2.497×10^{-5}	-1.687×10^{-4}
12	1.039×10^{-2}	-1.806×10^{-2}	-4.926×10^{-6}	1.654×10^{-4}
13	1.027×10^{-2}	1.806×10^{-2}	-2.497×10^{-5}	1.687×10^{-4}

Table 2

Relative Strain Energy Distribution

Mode	Element			
	1	2	3	4
1	1.00×10^{0}	1.03×10^{-1}	4.32×10^{-3}	1.52×10^{-3}
2	3.83×10^{-2}	5.96×10^{-2}	3.08×10^{-2}	4.32×10^{-3}
3	5.01×10^{-1}	1.74×10^{-2}	1.04×10^{-3}	1.01×10^{-3}
4	9.03×10^{-2}	3.06×10^{-3}	1.43×10^{-4}	1.02×10^{-4}

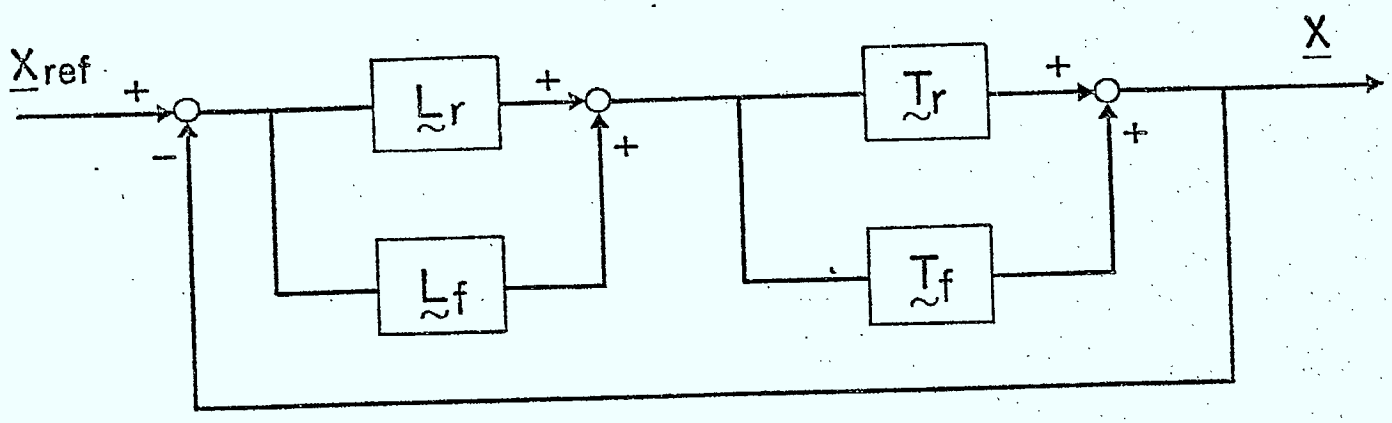

Figure 1(a) System Block Diagram

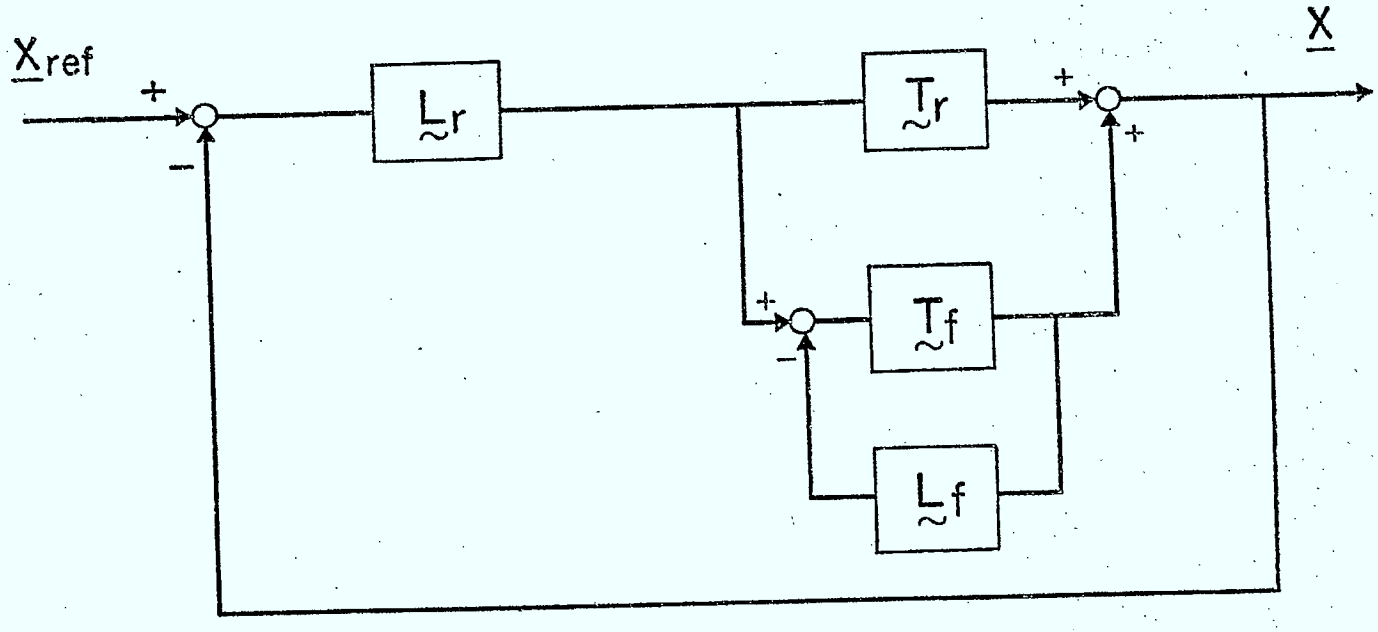

Figure 1(b) Simplified System Block Diagram

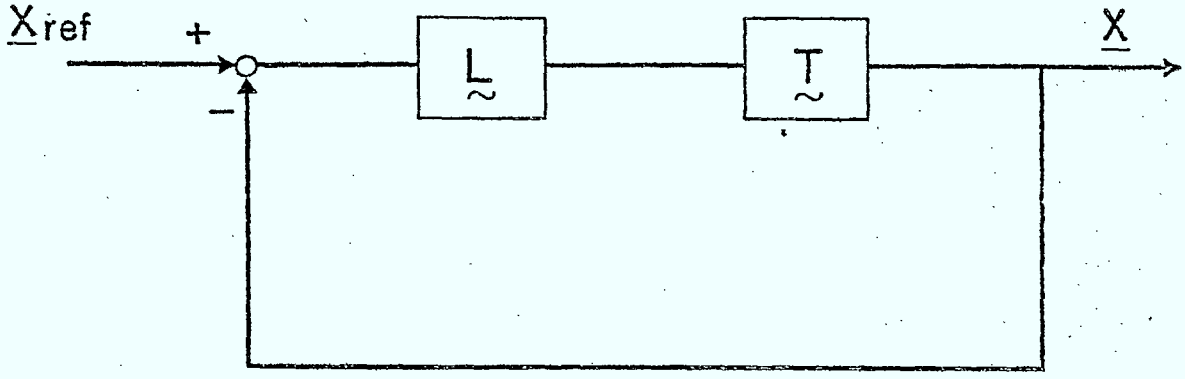

Figure 2 System Block Diagram Before Embedding

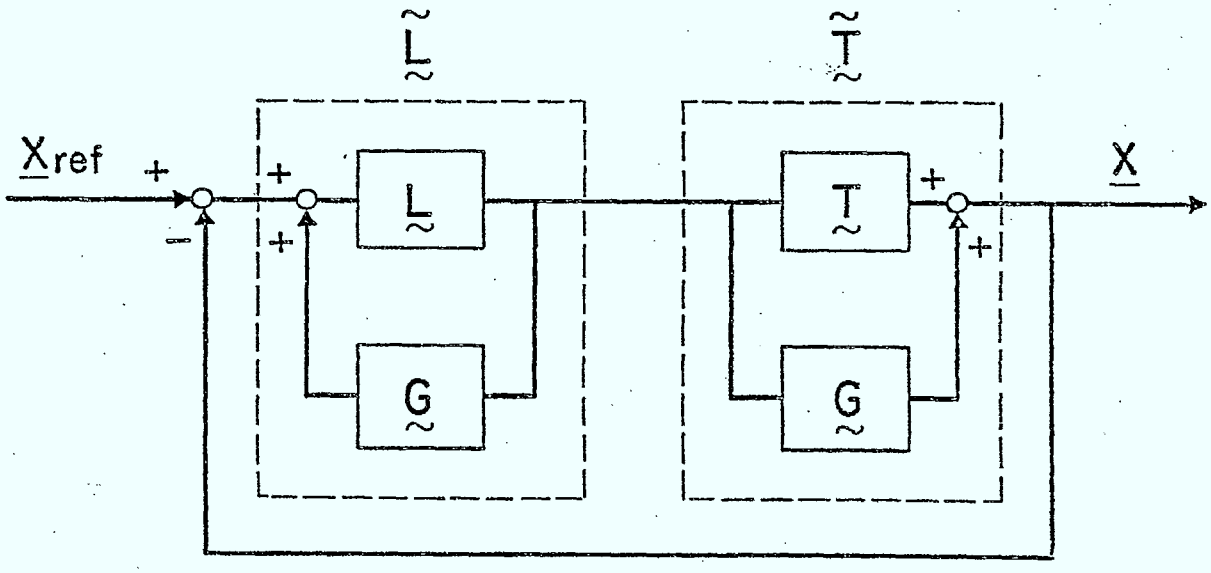

Figure 3 Equivalent System After Embedding

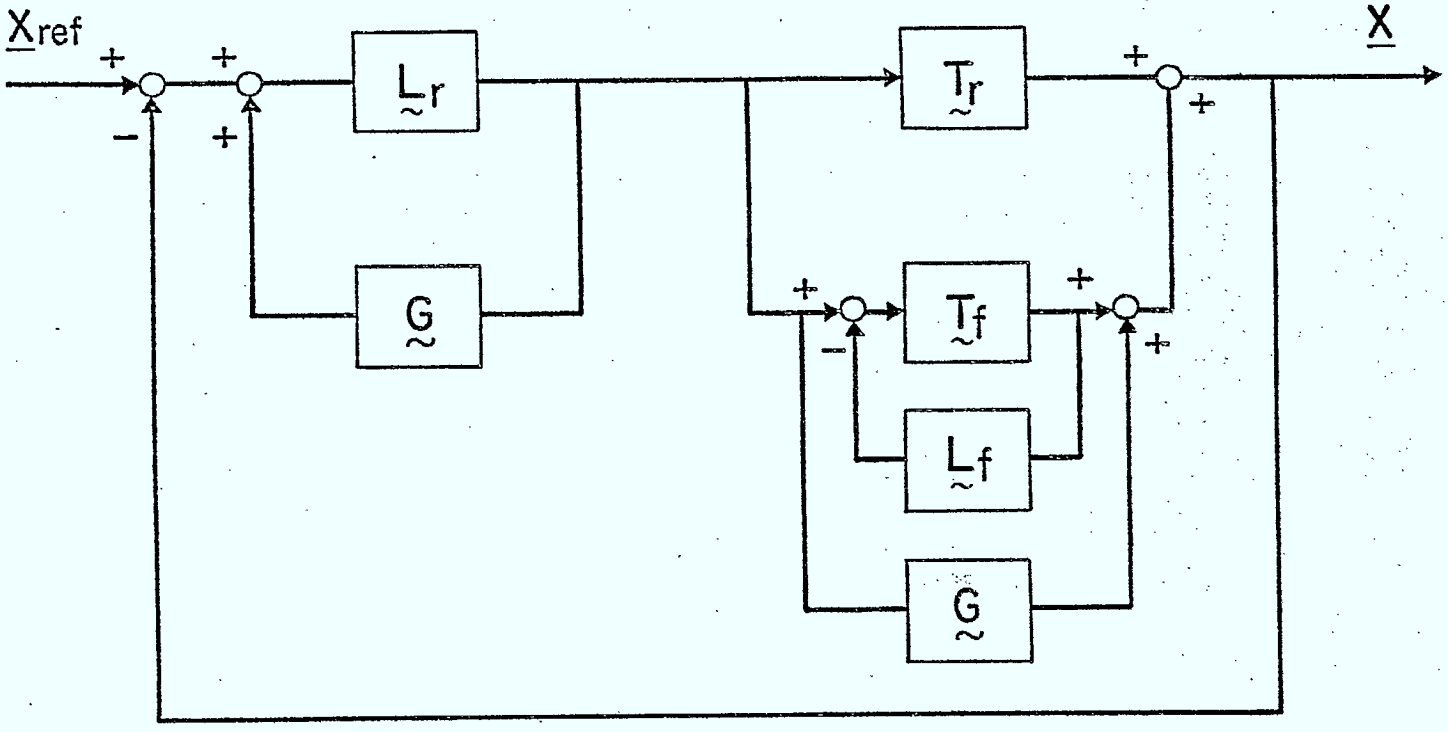

Figure 4 Equivalent System to Figure 1(b)

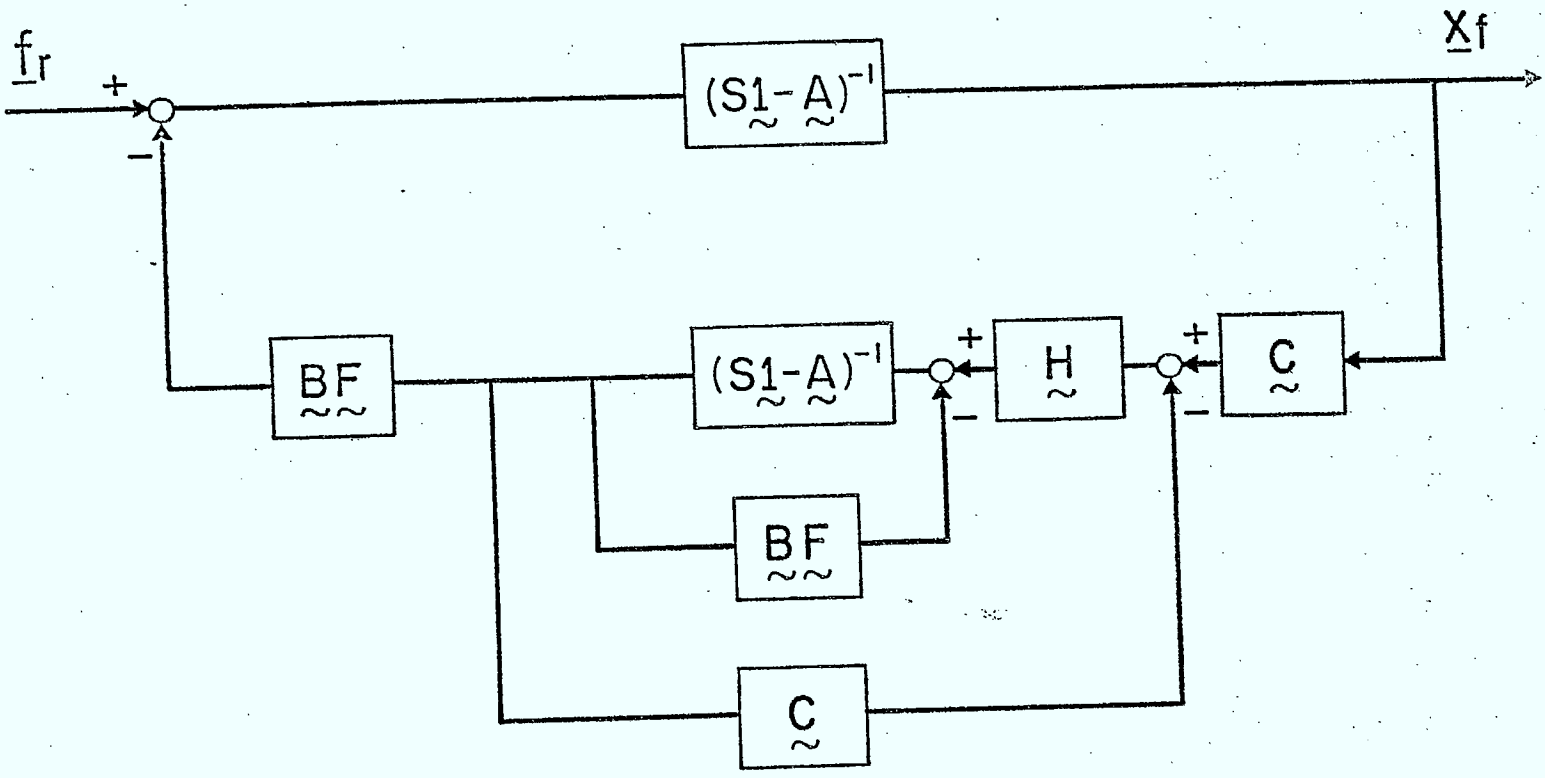

Figure 5 Output Feedback Block Diagram

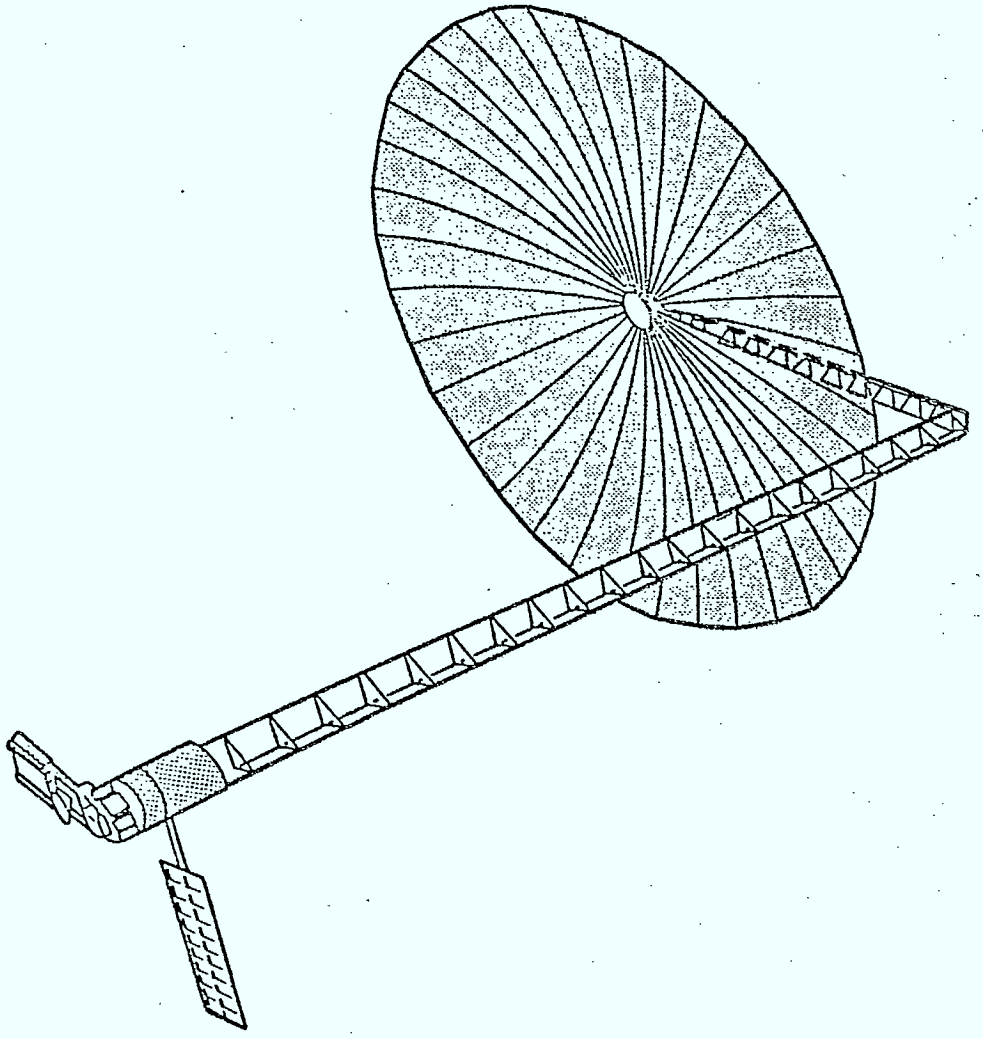

Figure 6(a) Mobile Communication Satellite

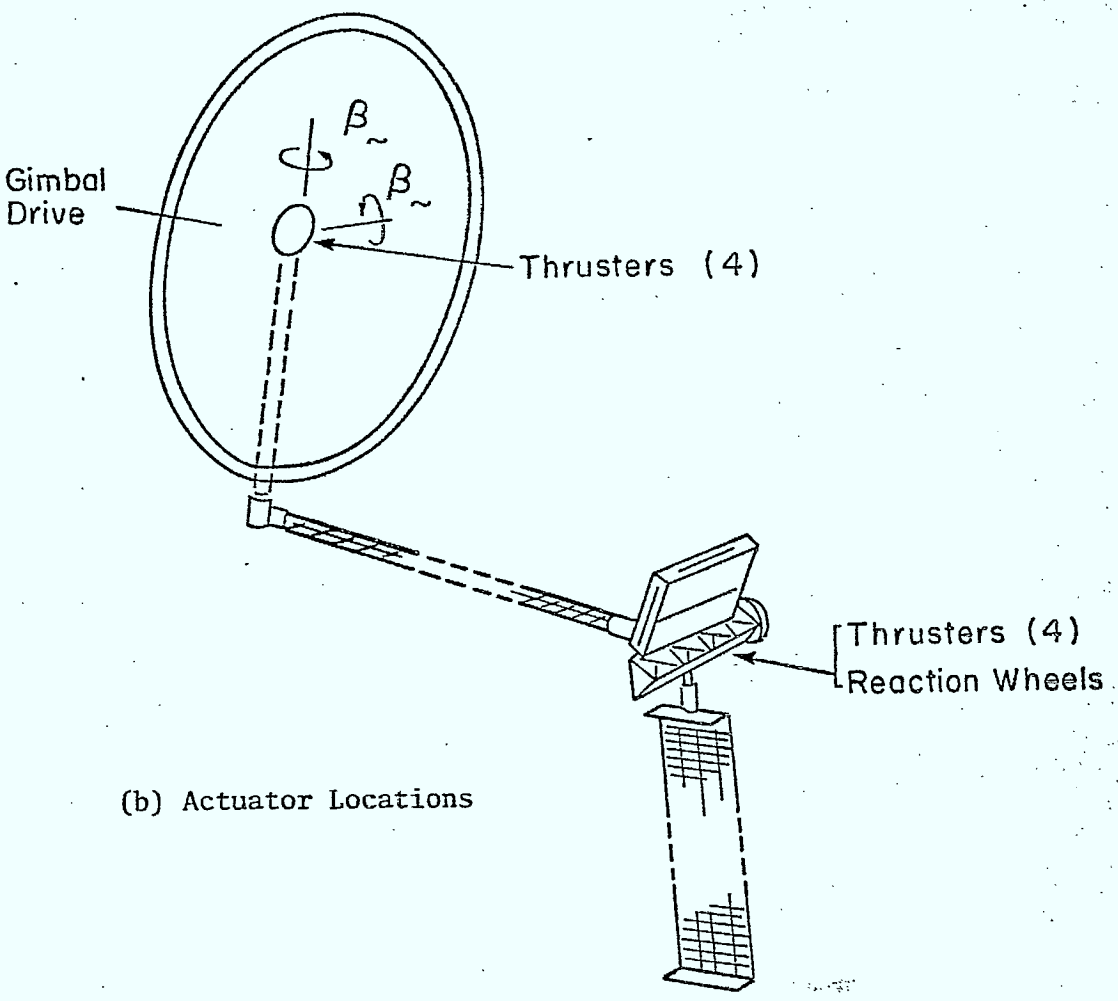

(b) Actuator Locations

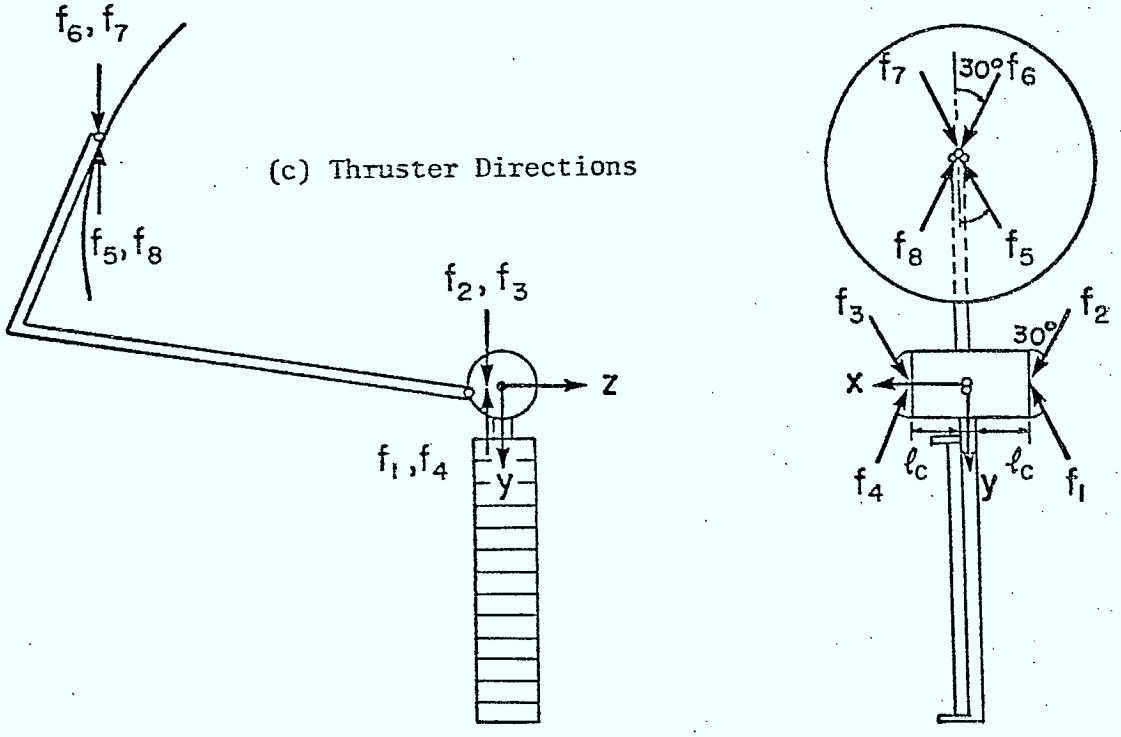

(c) Thruster Directions

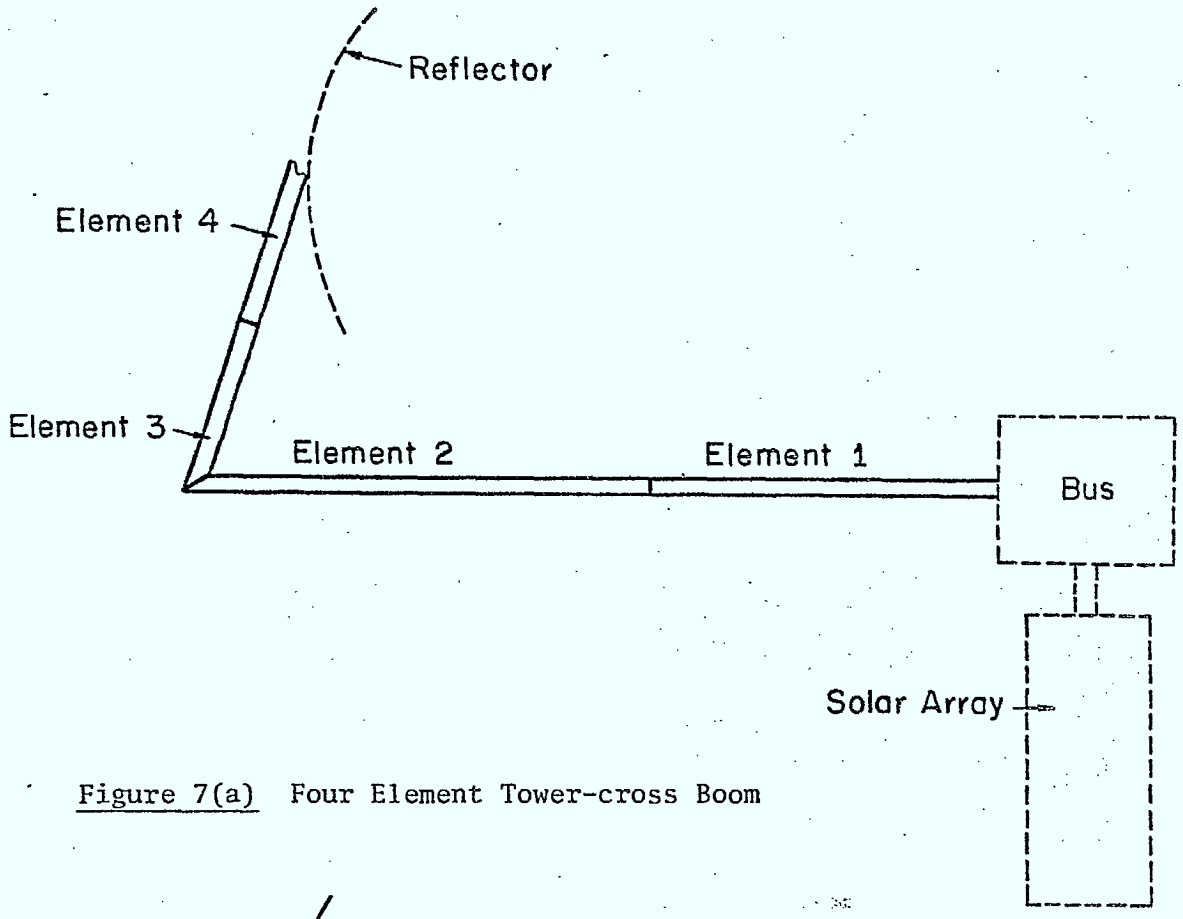

Figure 7(a) Four Element Tower-cross Boom

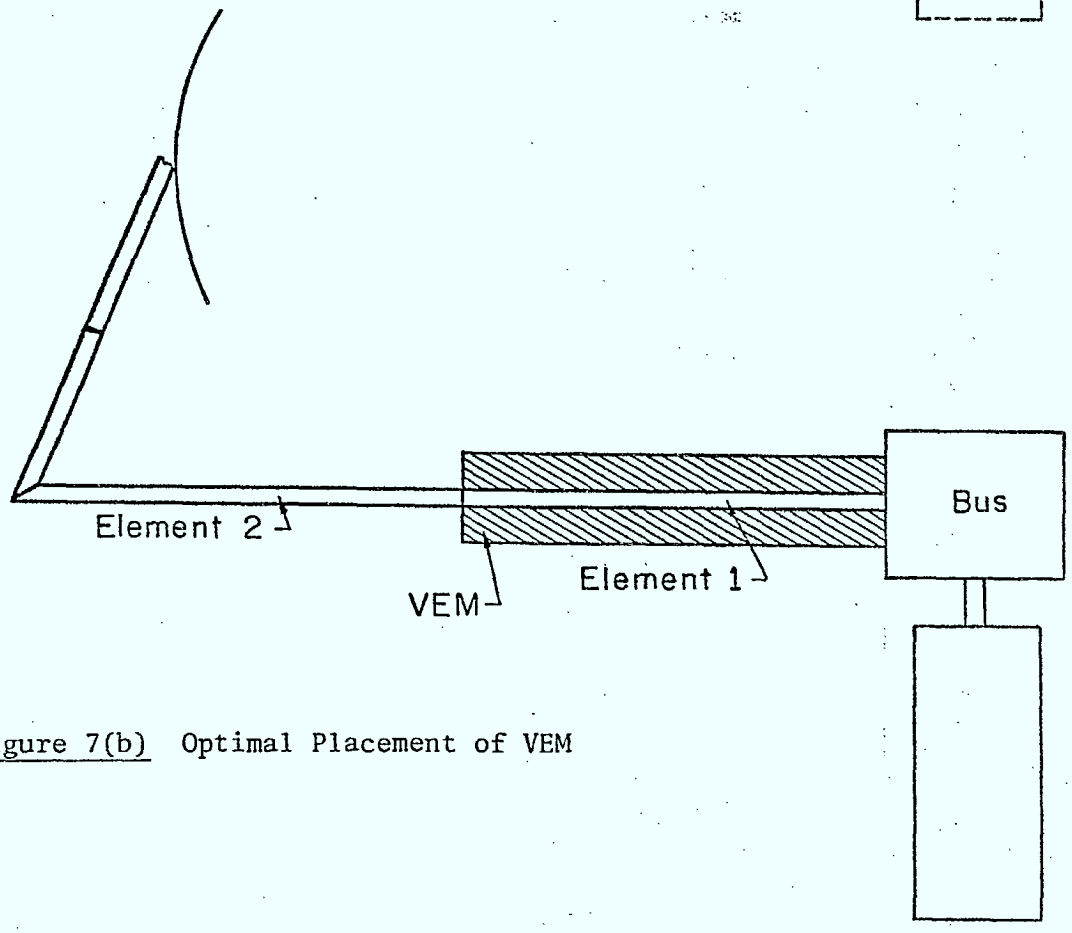

Figure 7(b) Optimal Placement of VEM

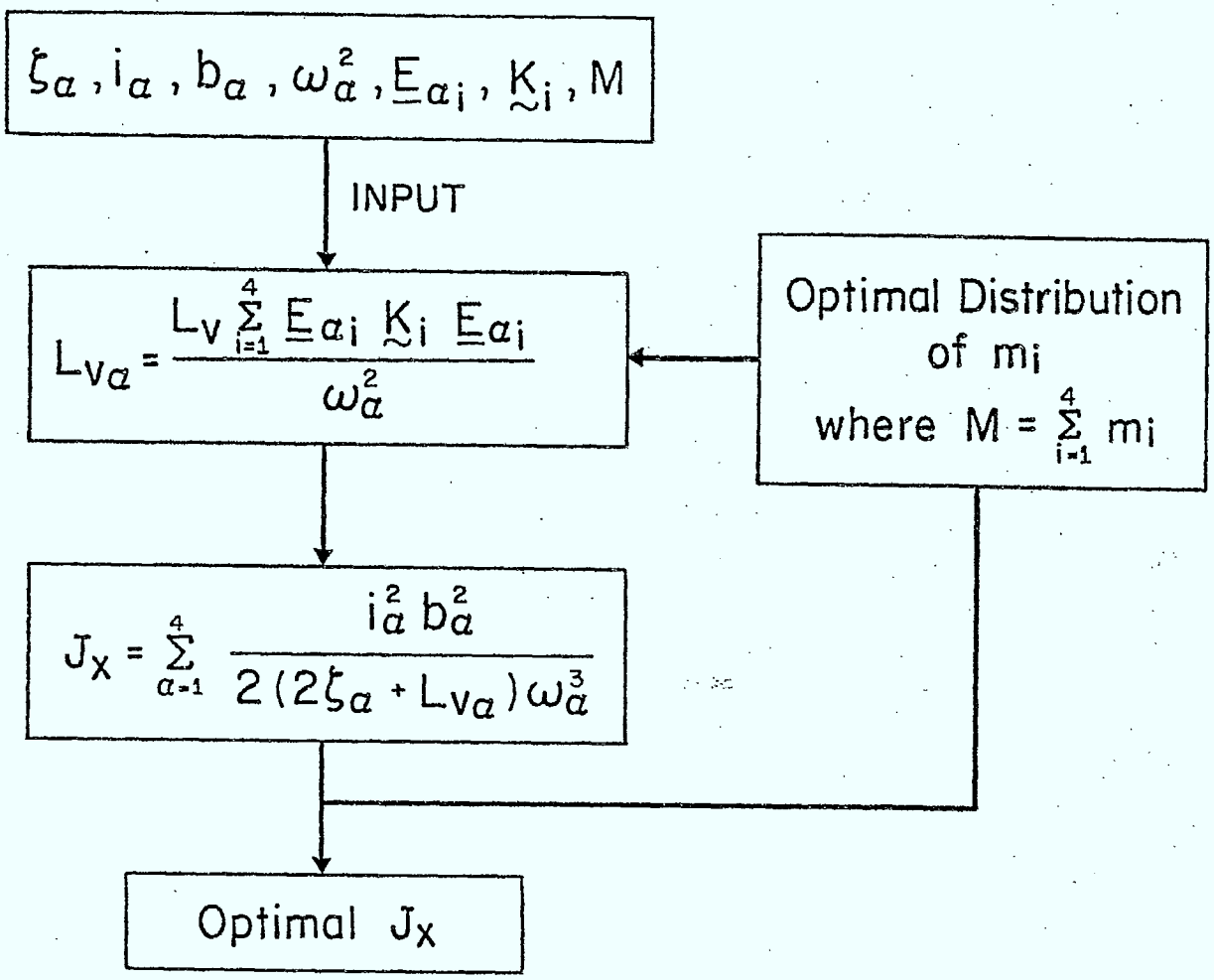

Note: i denotes element number

α denotes mode number

Figure 8 Flow Chart: Optimal Placement of VEM

Figures 9-11 Comparison of Weight-Cost Effectiveness Amongst Passive Damping, Active Damping with Kalman State Estimator - κ, and Active Damping with Full State Feedback.

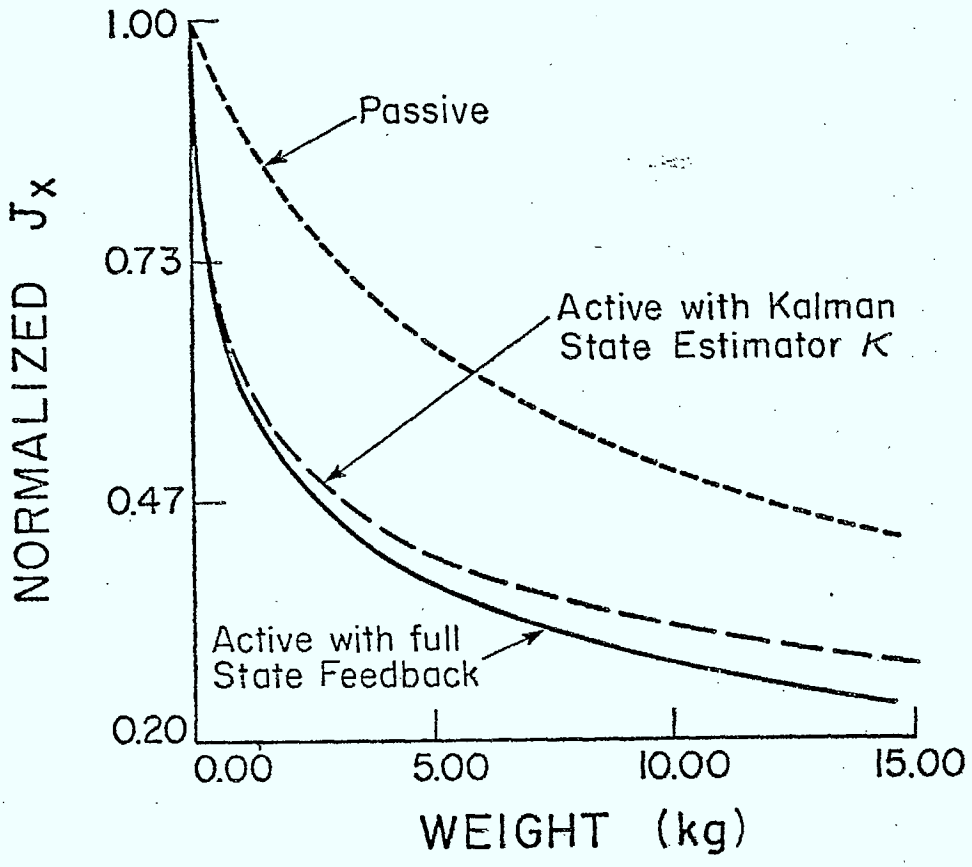

Figure 9 $\kappa = 10^3$

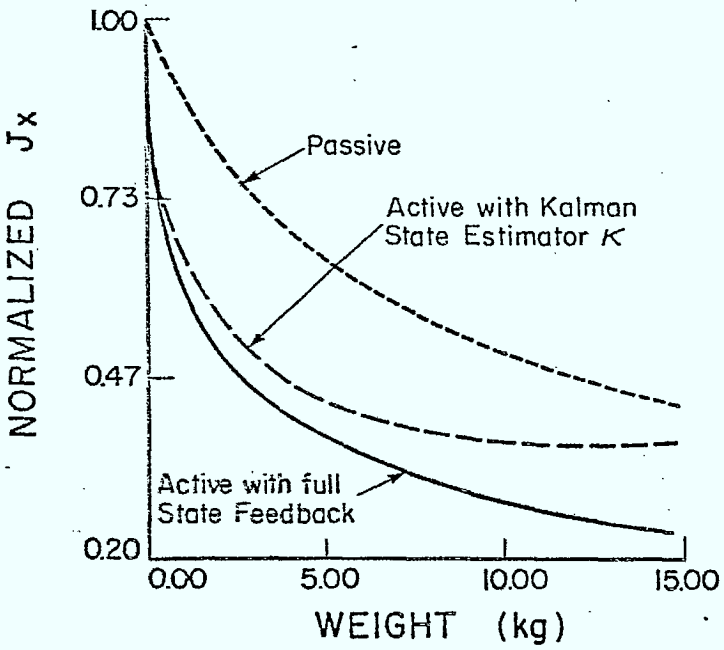

Figure 10 $\kappa = 10$

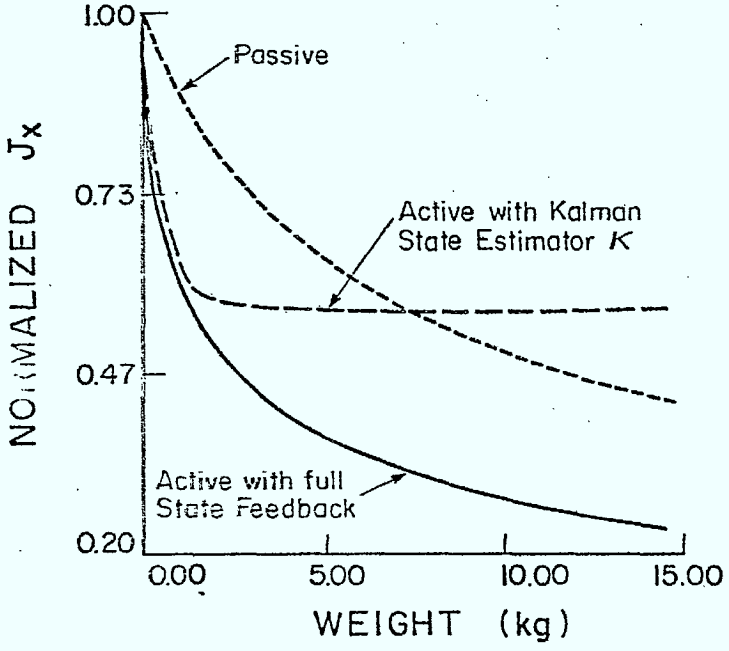

Figure 11 $\kappa = 2$

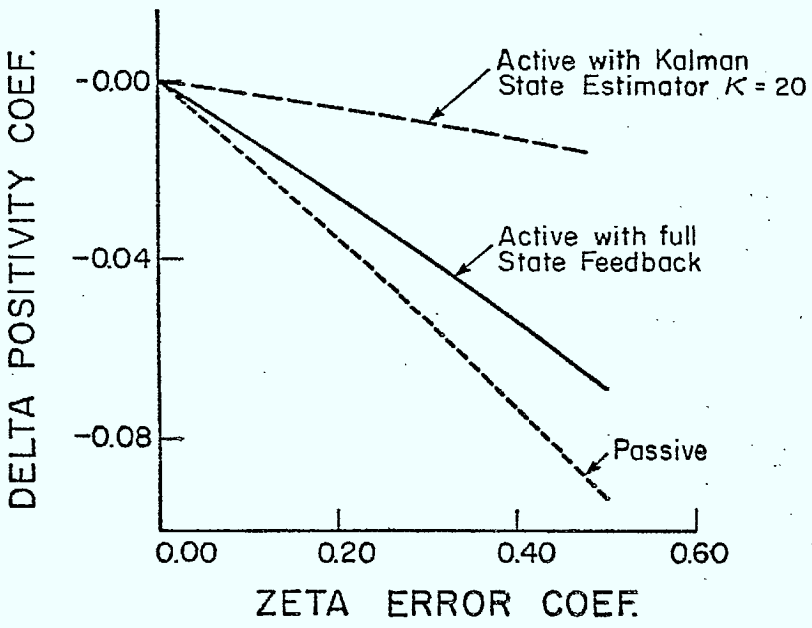

Figure 12 Positivity Comparison, M = 10 kg

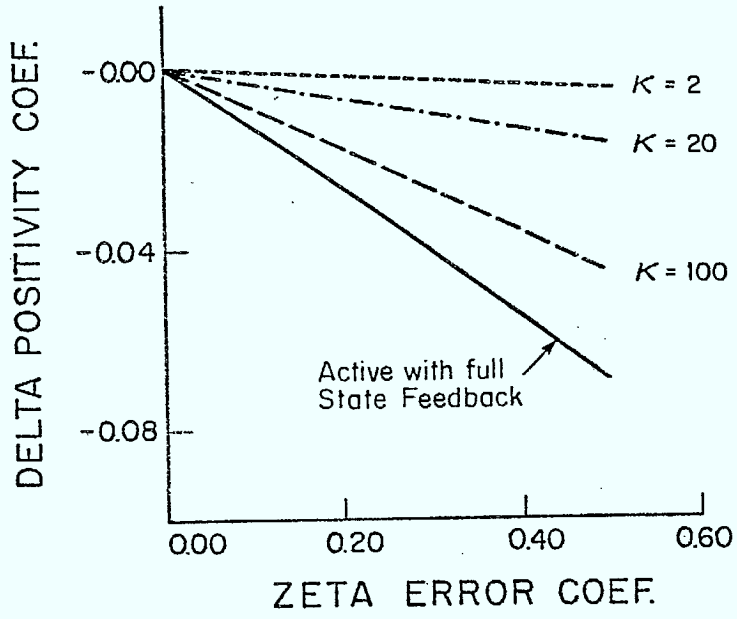

Figure 13 Positivity Comparison - Active Damping, M = 10 kg

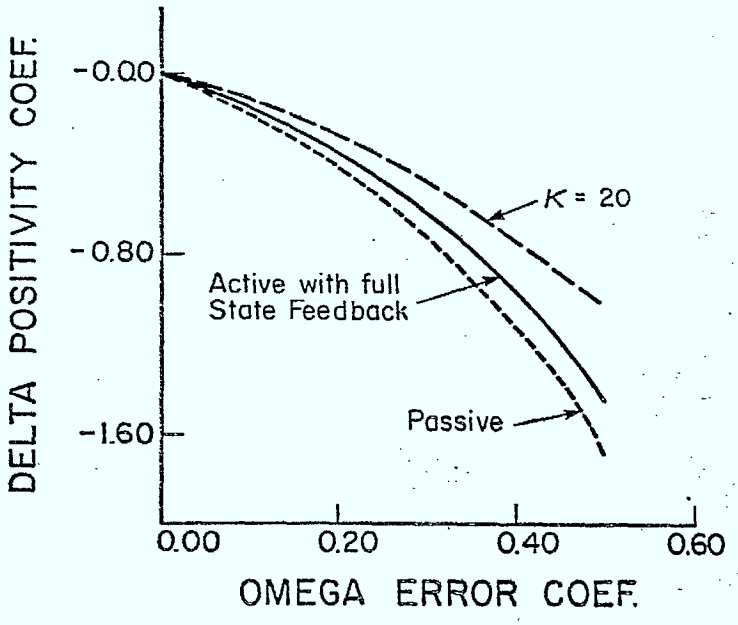

Figure 14 Positivity Comparison, M = 10 kg

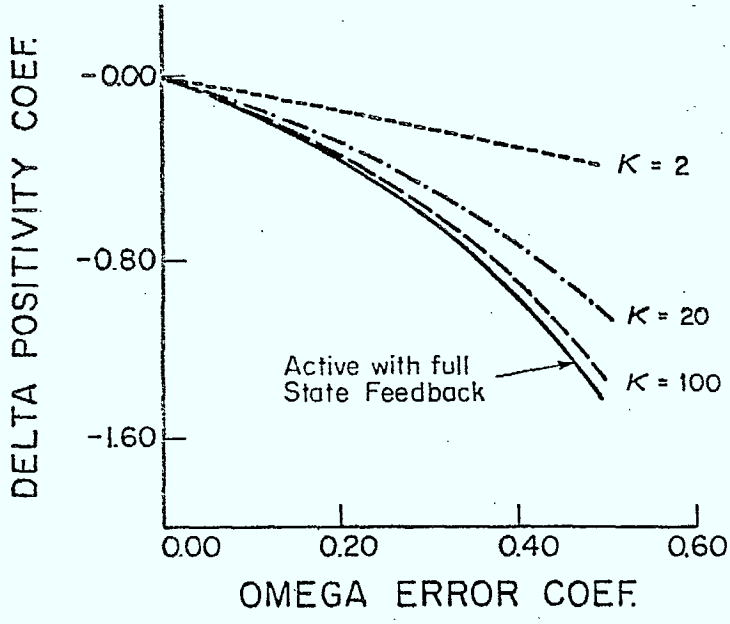

Figure 15 Positivity Comparison – Active Damping, M = 10 kg

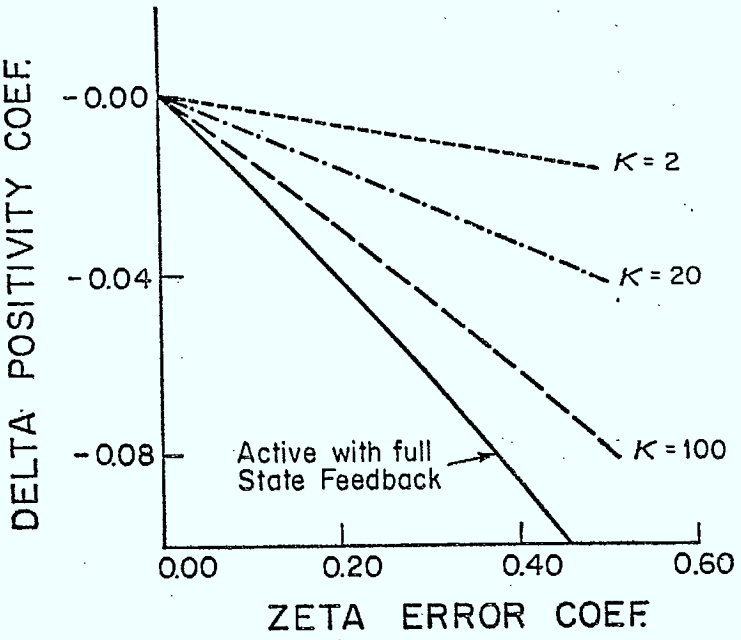

Figure 16 Active Damping Positivity Comparison, M = 5 kg

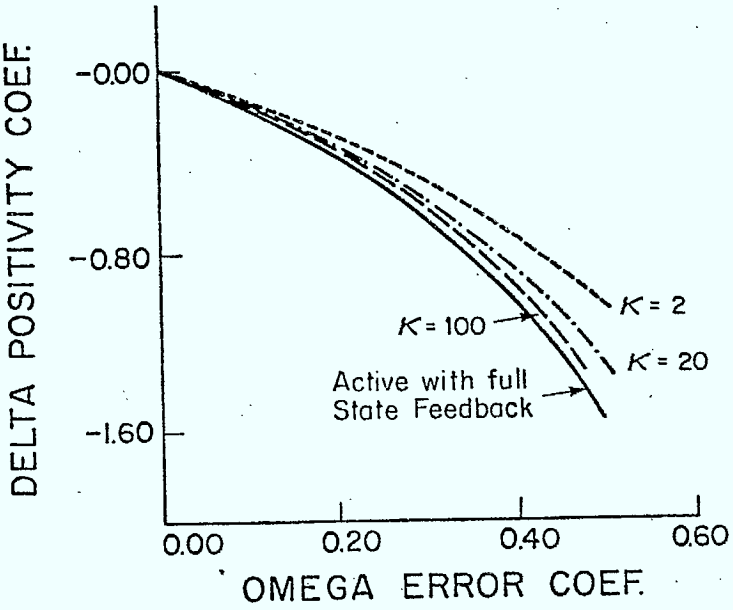

Figure 17 Active Damping Positivity Comparison, M = 5 kg

APPENDIX A

EQUIVALENT STABILITY CHARACTERISTICS

To prove that the transformation of the embedding technique maintains the stability characteristics of the original system, one need only examine their characteristic equations.

According to Figure 2, the closed-loop transfer matrix before embedding is given by

$$\underset{\sim}{T}_C = (\underset{\sim}{1} + \underset{\sim}{T}\,\underset{\sim}{L})^{-1}\underset{\sim}{T}\,\underset{\sim}{L} \tag{A-1}$$

After embedding (Figure 3), the closed-loop transfer matrix is

$$\underset{\sim}{\tilde{T}}_C = (\underset{\sim}{1} + \underset{\sim}{\tilde{T}}\,\underset{\sim}{\tilde{L}})^{-1}\underset{\sim}{\tilde{T}}\,\underset{\sim}{\tilde{L}} \tag{A-2}$$

where

$$\underset{\sim}{\tilde{T}} = \underset{\sim}{T} + \underset{\sim}{G} \tag{A.3a}$$

$$\underset{\sim}{\tilde{L}} = (\underset{\sim}{1} - \underset{\sim}{L}\,\underset{\sim}{G})^{-1}\underset{\sim}{L} \tag{A.3b}$$

Expanding (A-2) using (A-3) gives

$$\underset{\sim}{\tilde{T}}_C = [\underset{\sim}{1} + (\underset{\sim}{T} + \underset{\sim}{G})(\underset{\sim}{1} - \underset{\sim}{L}\,\underset{\sim}{G})^{-1}\underset{\sim}{L}]^{-1}(\underset{\sim}{T} + \underset{\sim}{G})(\underset{\sim}{1} - \underset{\sim}{L}\,\underset{\sim}{G})^{-1}\underset{\sim}{L} \tag{A-4}$$

$$= [(\underset{\sim}{1} - \underset{\sim}{L}\,\underset{\sim}{G})(\underset{\sim}{T} + \underset{\sim}{G})^{-1} + \underset{\sim}{L}]^{-1}\underset{\sim}{L} \tag{A-5}$$

Premultiply by $(\underset{\sim}{T} + \underset{\sim}{G})(\underset{\sim}{T} + \underset{\sim}{G})^{-1}$ to find

$$\underset{\sim}{T}_c = (\underset{\sim}{T} + \underset{\sim}{G})(\underset{\sim}{T} + \underset{\sim}{G})^{-1}[(\underset{\sim}{1} + \underset{\sim}{L}\,\underset{\sim}{G})(\underset{\sim}{T} + \underset{\sim}{G})^{-1} + \underset{\sim}{L})^{-1}\underset{\sim}{L} \qquad \text{(A-6)}$$

$$= (\underset{\sim}{T} + \underset{\sim}{G})(\underset{\sim}{1} + \underset{\sim}{T}\,\underset{\sim}{L})^{-1}\underset{\sim}{L} \qquad \text{(A-7)}$$

which has the same characteristic matrix equation as (A-1):

$$(\underset{\sim}{1} + \underset{\sim}{T}\,\underset{\sim}{L}) \qquad \text{(A-8)}$$

Therefore, the block diagram transformation has equivalent stability characteristics.

APPENDIX B

SIMPLIFICATION OF THE POSITIVITY INDEX

It is required to find the eigenvalues of

$$\underset{\sim}{T} = \underset{\sim}{T}(j\omega) + \underset{\sim}{T}^{H}(j\omega) \tag{B-1}$$

where

$$\underset{\sim}{T}(j\omega) = \underset{\sim}{C}(j\omega\underset{\sim}{1} - \underset{\sim}{A})^{-1}\underset{\sim}{C}^{T} \tag{B-2}$$

and $\underset{\sim}{A}$ and $\underset{\sim}{C}$ are real matrices.

Some simplification can be made to minimize computing costs.

$$\underset{\sim}{T} = \underset{\sim}{C}(j\omega\underset{\sim}{1} - \underset{\sim}{A})^{-1}\underset{\sim}{C}^{T} + [\underset{\sim}{C}(j\omega\underset{\sim}{1} - \underset{\sim}{A})^{-1}\underset{\sim}{C}^{T}]^{H} \tag{B-3}$$

Since $\underset{\sim}{C}^{T} = \underset{\sim}{C}^{H}$, then

$$\underset{\sim}{T} = \underset{\sim}{C}[(j\omega\underset{\sim}{1} - \underset{\sim}{A})^{-1} + (j\omega\underset{\sim}{1} - \underset{\sim}{A})^{-H}]\underset{\sim}{C}^{T} \tag{B-4}$$

Now

$$(j\omega - \underset{\sim}{A})^{-1} = -\underset{\sim}{N}(j\omega\underset{\sim}{1} + \underset{\sim}{A}) \tag{B-5}$$

$$(j\omega - \underset{\sim}{A})^{-H} = -(j\omega\underset{\sim}{1} + \underset{\sim}{A})^{H}\underset{\sim}{N}^{T} \tag{B-6}$$

where

$$\underset{\sim}{N} = (\omega^{2}\underset{\sim}{1} - \underset{\sim}{A}\,\underset{\sim}{A})^{-1} \tag{B-7}$$

Also note that

$$(j\omega\underset{\sim}{1} - \underset{\sim}{A})^{H} = (-j\omega\underset{\sim}{1} + \underset{\sim}{A}^{T}) \tag{B-8}$$

Therefore, substituting (B-5, 6, 8) into (B-4) gives

$$\underset{\sim}{T} = \underset{\sim}{C}[-\underset{\sim}{N}(j\omega\underset{\sim}{1} + \underset{\sim}{A}) + (j\omega\underset{\sim}{1} - \underset{\sim}{A}^T)\underset{\sim}{N}^T]\underset{\sim}{C}^T \qquad \text{(B-9)}$$

or

$$\underset{\sim}{T} = \underset{\sim}{C}[-\underset{\sim}{N}\,\underset{\sim}{A} - (\underset{\sim}{N}\,\underset{\sim}{A})^T + j\omega(\underset{\sim}{N}^T - \underset{\sim}{N})]\underset{\sim}{C}^T \qquad \text{(B-10)}$$

Noting that $\underset{\sim}{N}^T - \underset{\sim}{N}$ is skew-symmetric, $\underset{\sim}{T}$ can be computer coded quite efficiently.

SHEN, FRANCIS
A quantitative comparison of active and passive damping for large space structures